A Deep Learning Framework for Medium-Term Covariance Forecasting in Multi-Asset Portfolios[*]

Pedro Reis,[†] Ana Paula Serra[‡] and João Gama[§]

arXiv:2503.01581v2 [cs.CE] 15 Apr 2025

[†]University of Porto, School of Economics and Management and Center for Economics and Finance (cef.up), R. Dr Roberto Frias 46, 4200-464 Porto, Portugal; and INESCTEC, Campus da Faculdade de Engenharia da Universidade do Porto, R. Dr. Roberto Frias, 4200-465 Porto, Portugal. Email: pdreis1988@gmail.com

[‡]University of Porto, School of Economics and Management and Center for Economics and Finance (cef.up), R. Dr Roberto Frias 46, 4200-464 Porto, Portugal.

[§]INESCTEC, Campus da Faculdade de Engenharia da Universidade do Porto, R. Dr. Roberto Frias, 4200-465 Porto, Portugal.

Abstract

Accurate covariance forecasting is central to portfolio allocation, risk management, and asset pricing, yet many existing methods struggle at medium-term horizons, where shifting market regimes and slower dynamics predominate. We propose a deep learning framework that combines three-dimensional convolutional neural networks, bidirectional long short-term memory layers, and multi-head attention to capture complex spatio-temporal dependencies. Using daily data on 14 exchange-traded funds from 2017 through 2023, we find that our model reduces Euclidean and Frobenius distance metrics by up to 20% relative to classical benchmarks (e.g., shrinkage and GARCH approaches) and remains robust across distinct market regimes. Our portfolio experiments demonstrate significant economic value through lower volatility and moderate turnover. These findings highlight the potential of advanced deep learning architectures to improve medium-term covariance forecasts, offering practical benefits for institutional investors and risk managers.

Keywords: Covariance Matrix Forecasting, Deep Learning, Portfolio Optimisation, Medium-Term Horizons, Financial Markets.
JEL codes: C45, G11, G17.

1 Introduction

Covariance matrix forecast is central in modern finance. It influences portfolio construction, risk management, and asset pricing models. Markowitz (1952) introduced mean-variance optimisation, highlighting how correlation among assets shapes the risk-return trade-off. Beyond portfolio choice, covariance forecast underpins factor-based models, hedging strategies, and even debates on market efficiency, where accurate correlation forecasts can drive risk control and potential outperformance.

Early studies found that even simple correlation structures could improve capital allocation. For instance, Elton and Gruber (1973) suggested using constant-correlation estimates over historical windows for a decade. Their work showed that stable or slowly changing correlation patterns can help avoid distortions caused by transient market fluctuations.

Over time, multiple research strands have focused on short-horizon covariance forecasts. High-frequency datasets, such as intraday prices, enable detailed volatility analyses, often using generalised autoregressive conditional heteroskedasticity (GARCH) based models. Constant (Bollerslev, 1990) and dynamic conditional correlation (Engle, 2002) specifications remain common benchmarks, although Symitsi et al. (2018) argue that little fundamental progress has been made recently. Extensions include applying the heterogeneous autoregressive model (Corsi, 2009) in a multivariate setting through Cholesky decomposition[1] (Chiriac and Voev, 2011). However, the Cholesky decomposition models outperform DRD-based[2] (Bollerslev et al., 2018).

However, GARCH-type approaches struggle with large cross-sections, falling prey to the curse of dimensionality (Engle et al., 2019). Tools like principal component analysis and random matrix theory (Ledoit and Wolf, 2003; Laloux et al., 2000) have been effective for large datasets. Recent advances, such as dynamic conditional correlation with nonlinear shrinkage (Engle et al., 2019), perform well overall, as per De Nard et al. (2024). Still, most of these methods focus on very short-term horizons, often just one step ahead or one day ahead, and rely on high-frequency data.

---

[1]Cholesky decomposition is a method that breaks down a positive definite matrix into the product of a lower triangular matrix and its transpose.

[2]Dynamic Relationship/Dependence (DRD) models refer to time-varying models that separate covariance into volatility and correlation components forecasts.

Long-horizon forecasts matter for institutional investors, such as pension and investment funds. They rebalance portfolios over weeks or months. Therefore, a one-step forecast is insufficient for practical decision-making (De Nard et al., 2022). Furthermore, slow-moving trends, such as equity–bond correlation shifts, can be overlooked if one relies solely on high-frequency econometric models. Sandoval and Franca (2012) highlights how regime shifts or significant structural changes often go undetected in classical specifications, raising the risk of large drawdowns and poor capital allocation.

For longer-term horizons, naive and factor models are more common (Ledoit and Wolf, 2004; De Nard et al., 2022). Factor models can provide insightful forecasts but may not generalise well across diverse portfolios, especially when different portfolios are affected by many different factors. These methods are typically stable but can underperform when major shifts occur.

Naive approaches assume that recent covariance estimates strongly predict future covariances as they follow a Markov process. However, these tend to be noisy when the number of assets tends to be close to the number of observations ($N \approx T$). For this purpose, shrinkage techniques reduce noise by blending the sample covariance matrix with structured targets, particularly when the cross-section of assets is large (Ledoit and Wolf, 2022).

While these methods rely on advanced statistical and econometric methods, we have seen a recent surge in machine learning methods that can also handle non-linearities and high dimensionality with more accurate forecast. Gu et al. (2020) and Kim et al. (2023) use techniques like random forests, support vector machines, and generative adversarial networks, while Zhang et al. (2024) applies graph neural networks to capture volatility spillovers for covariance matrix forecast. However, most of these solutions still emphasise short-term horizons.

Attention mechanisms (Vaswani et al., 2017) offer a promising direction by weighting key observations more heavily. Some studies apply these techniques in finance but still focus on short-horizon tasks (Nazaret and Reddy, 2023; Olorunnimbe and Viktor, 2023). In principle, attention-based models could capture the slow-moving, cyclical factors and abrupt shifts that define medium- and long-horizon covariance forecasts, realising this potential. However, it requires integrating sophisticated data-driven architectures with the economic logic of excess returns.

Recent efforts to extend these approaches to multi-asset portfolios have been limited. While many studies handle large cross-sections of stocks or focus on single-asset classes (Reis et al., 2024), fewer examine the combined dynamics across multiple asset classes in an integrated framework. However, institutional investors routinely diversify across equities, bonds, alternatives, and

derivatives, underscoring the need for robust, multi-asset covariance forecasting models. In particular, capturing time-varying cross-asset correlations over medium-term horizons is a non-trivial challenge that remains under-explored in much of the existing literature.

Two key research gaps remain. First, most existing studies focus on short- or long-term horizons, leaving a relative void in medium-term covariance forecasting. This gap is particularly salient for multi-asset portfolios, where cross-asset correlations over multi-week or multi-month windows can significantly influence asset allocation and risk management (De Nard et al., 2021). Second, there is limited empirical evidence on whether using *raw* returns versus *excess* returns leads to systematically different covariance forecasts, especially over these medium-term horizons. Economic theory suggests that underlying drivers of asset co-movements could be more accurately captured through *excess* returns (Fama and French, 1993), i.e. by removing the risk-free component from returns. However, most machine learning and econometric approaches mostly default to *raw* returns.

Our study addresses these gaps by focusing on medium-term covariance forecasts in a multi-asset setting. Specifically, we propose a novel deep learning (DL) model that captures spatio-temporal correlations while remaining robust to structural changes. We benchmark against classical methods and demonstrate consistent gains in forecast accuracy under diverse market environments from 2017 to 2023. Our main contributions are as follows:

- We present an integrated 3D-convolution neural network (CNN) and bidirectional long-short-term memory (LSTM) architecture with multi-head attention that improves medium-term forecasting accuracy.

- We compare different return-processing specifications (including the treatment or omission of risk-free rates) and show that the proposed approach preserves its predictive edge.

- We evaluate the economic value of our forecasts in a global minimum-variance (GMV) portfolio, demonstrating significant variance reduction and stable turnover.

The rest of the paper is structured as follows. Section 2 introduces the benchmark methods and our DL model. Section 3 presents the main empirical findings. Section 4 reports robustness checks. Section 5 explores implications for portfolio management. Finally, Section 6 concludes.

2 Methodology

Let $\mathbf{r}_t$ denote the N-dimensional row vector of excess daily returns for N assets at time t. Assuming time-varying mean excess returns, $\mathbf{r}_t$ can be expressed as follows:

$$\mathbf{r}_t = \boldsymbol{\mu}_t + \mathbf{e}_t \tag{1}$$

where $\boldsymbol{\mu}_t$ is the N-dimensional vector of rolling means of the excess daily returns, and $\mathbf{e}_t$ is the i.i.d. error terms with a normal distribution within each rolling window:

$$\mathbf{e}_t \sim N\left(\mathbf{0}, \boldsymbol{\Sigma}_t\right) \tag{2}$$

Although empirical evidence suggests financial returns often exhibit heavy tails and non-zero skewness (Cont, 2001), we adopt the normality assumption because it is standard in many benchmark models (e.g., GARCH-based correlation models and Ledoit–Wolf shrinkage). However, we acknowledge that alternative distributions (e.g., Student-t innovations, mixture models, or those explicitly modelling tail dependence) may better capture extreme events and skewness in practice[3] (Hansen, 1994; Harvey, 1997).

The rolling mean $\boldsymbol{\mu}_t$ and rolling standard deviation $\boldsymbol{\sigma}_t$ at time t are calculated using a window of size F as follows:

$$\boldsymbol{\mu}_t = \frac{1}{F} \sum_{k=t-F+1}^{t} \mathbf{r}_k \tag{3}$$

$$\boldsymbol{\sigma}_t^2 = \frac{1}{F-1} \sum_{k=t-F+1}^{t} \left(\mathbf{r}_k - \boldsymbol{\mu}_t\right) \odot \left(\mathbf{r}_k - \boldsymbol{\mu}_t\right) \tag{4}$$

where $\odot$ denotes the element-wise product. Therefore, the realised covariance matrix ($\boldsymbol{\Sigma}_t$) is an

---

[3]Extending our DL framework to accommodate such heavy-tailed or asymmetric distributions is an area for future research. Nevertheless, our empirical results in subsequent sections suggest that even a normality-based design can significantly enhance covariance forecasts, given the robustness of the data-driven layers in handling complex, nonlinear dependencies.

$N \times N$ matrix with each element calculated as:

$$Cov_t \left(\mathbf{r}_i, \mathbf{r}_j \right) = \frac{1}{F-1} \sum_{k=t-F+1}^{t} \left(r_{i,k} - \mu_{i,t} \right) \left(r_{j,k} - \mu_{j,t} \right) \tag{5}$$

Our goal is to estimate the conditional covariance matrix of the asset returns for the next F days based on the information available at time t:

$$\widehat{\boldsymbol{\Sigma}}_{t+1:t+F} = Cov \left(\mathbf{r}_{t+1}, \mathbf{r}_{t+2}, \ldots, \mathbf{r}_{t+F} | \mathcal{F}_t \right) \tag{6}$$

where $\mathcal{F}_t$ is the sigma-algebra representing all the information available at time t.

To estimate $\widehat{\boldsymbol{\Sigma}}_{t+1:t+F}$, we compare 10 benchmark models divided into three groups (naive, de-noising and GARCH models) alongside our proposed model. A description of each model is shown below.

2.1 Naïve Models

2.1.1 Naïve (NA)

A naive covariance forecasting approach is based on the lagged realised covariance. This model assumes that covariance is a Markov process, so the covariance matrix of the previous period is highly informative about the future covariance matrix. Under this model:

$$\widehat{\boldsymbol{\Sigma}}_{t+1:t+F} = \boldsymbol{\Sigma}_{t-F:t} \tag{7}$$

This forecasting method is as simple as possible as it requires no optimisation.

2.1.2 Naïve full sample (NA^F)

Another naïve technique is to use the full sample instead of the rolling covariance matrix as our estimator.

$$\widehat{\boldsymbol{\Sigma}}_{t+1:t+F} = \boldsymbol{\Sigma} \tag{8}$$

where $\boldsymbol{\Sigma}$ is the covariance matrix of our sample up until t.

2.1.3 Exponential Weighted Moving Average ($EWMA$)

The EWMA employs exponentially decaying weights for the covariance matrix. The covariance matrix in the EWMA model is recursively computed as follows:

$$\widehat{\boldsymbol{\Sigma}}_{t+1:t+F} = (1-\eta)\mathbf{e}_t\mathbf{e}_t^{'} + \eta\boldsymbol{\Sigma}_{t-F:t} \tag{9}$$

where $\mathbf{e}_t$ is the N-dimensional vector of the error terms of all assets from Eq. (1), at time t, and η acts as a decay factor, confined within the range [0,1], dictating the rate at which the weights on past observations decrease. This factor has been approximated to be around 0.94 (J.P.Morgan, 1996).

2.2 De-noising Models

2.2.1 Principal Component Analysis (PCA)

As noted by Ledoit and Wolf (2003), empirical results show the usefulness of PCA in covariance matrix forecast. The PCA is computed as follows:

$$\widehat{\boldsymbol{\Sigma}}_{t+1:t+F} = \mathbf{U}\boldsymbol{\Lambda}\mathbf{U}^{\top} \tag{10}$$

where $\mathbf{U}$ is the matrix of eigenvectors and $\boldsymbol{\Lambda} = \text{diag}(\lambda_1, \lambda_2, ..., \lambda_N)$ is the diagonal matrix of eigenvalues.

To ensure we capture most of the information, we retain only the first k principal components that account for at least 95% of the total variance. This is expressed as:

$$\sum_{i=1}^{k}\lambda_i \geq 0.95\sum_{i=1}^{N}\lambda_i \tag{11}$$

The final forecasted covariance matrix is then approximated as:

$$\widehat{\boldsymbol{\Sigma}}_{t+1:t+F} \approx \mathbf{U}_k\boldsymbol{\Lambda}_k\mathbf{U}_k^{\top} \tag{12}$$

2.2.2 Random Matrix Theory (RMT)

RMT (Laloux et al., 2000) is built upon the PCA where the upper (λ_+) and lower (λ_-) bound of the eigenvalues are calculated using the Marchenko-Pastur distribution. These bounds are calculated as:

$$\lambda_+ = \left(1 + \frac{1}{\sqrt{q}}\right)^2, \quad \lambda_- = \left(1 - \frac{1}{\sqrt{q}}\right)^2 \tag{13}$$

where $q = T/N$ is the ratio of the window size to the number of assets. Eigenvalues within these bounds are dominated by noise, while eigenvalues outside the bounds represent meaningful information.

$$\lambda_i^{\text{filtered}} = \begin{cases} \lambda_i & \text{if } \lambda_i > \lambda_+ \text{ or } \lambda_i < \lambda_- \\ \frac{\lambda_+ + \lambda_-}{2} & \text{otherwise} \end{cases} \tag{14}$$

This filtering process removes noise and retains only the significant components of the covariance matrix. The cleaned covariance matrix is reconstructed by multiplying the filtered eigenvalues ($\mathbf{\Lambda}^{\text{filtered}}$) with their corresponding eigenvectors:

$$\widehat{\mathbf{\Sigma}}_{t+1:t+F} = \mathbf{U}\mathbf{\Lambda}^{\text{filtered}}\mathbf{U}^\top \tag{15}$$

2.2.3 Ledoit and Wolf (LW)

The LW shrinkage (Ledoit and Wolf, 2004) is a robust statistical model that combines the sample covariance matrix with a structured target matrix, improving forecast accuracy by reducing the impact of forecast error due to high dimensionality and limited sample size. The LW shrinkage estimator is given by:

$$\widehat{\mathbf{\Sigma}}_{t+1:t+F} = \rho\mathbf{T} + (1 - \rho)\mathbf{\Sigma}_{t-F:t} \tag{16}$$

where $\mathbf{T} = \frac{\text{Tr}(\mathbf{\Sigma}_{t-F:t})}{N} \times \mathbf{I}$ is the target matrix, with $\mathbf{I}$ being the identity matrix and $\text{Tr}(\mathbf{\Sigma}_{t-F:t})$ representing the sum of the diagonal elements of the sample covariance matrix. The shrinkage coefficient ρ is optimally determined to minimise the mean squared error between the estimated and true covariance matrices:

$$\rho = \frac{\sum_{i \neq j} \text{Var}(\sigma_{i,j})}{\sum_{i \neq j}(\sigma_{i,j} - t_{i,j})} \tag{17}$$

where $\sigma_{i,j}$ are the elements of the sample covariance matrix and $t_{i,j}$ are the elements of the target matrix $\mathbf{T}$.

2.2.4 Ledoit and Wolf full sample (LW^F)

Similarly to the NA^F model, we employed a full sample of Ledoit and Wolf (2004) as a shrinkage model.

$$\widehat{\Sigma}_{t+1:t+F} = \rho \mathbf{T} + (1 - \rho)\mathbf{\Sigma} \tag{18}$$

2.3 GARCH Models

2.3.1 Constant Conditional Correlations (CCC)

The CCC model, introduced by Bollerslev (1990), assumes that asset correlations remain constant over time while variances evolve dynamically according to a GARCH process based on a one-step forecast. To extend the model to a multi-step forecasting framework, we follow the methodology of Baillie and Bollerslev (1992), defining the F-step ahead conditional covariance forecast as:

$$\widehat{\Sigma}_{t+1:t+F} = \frac{1}{F} \sum_{f=1}^{F} \mathbf{D}_{t+f} \mathbf{R} \mathbf{D}_{t+f}, \tag{19}$$

where $\mathbf{D}_{t+f} = \text{diag}\left(\sqrt{h_{11,t+f}}, \sqrt{h_{22,t+f}}, \ldots, \sqrt{h_{NN,t+f}}\right)$ is the diagonal matrix of forecasted conditional volatilities for horizon f and R the conditional correlation matrix. The multi-step averaging approach used in Eq. (19) was introduced by De Nard et al. (2021) to provide a more stable covariance forecast over the rebalancing period. The $h_{ii,t}$ series is modelled using univariate GARCH(1,1) processes:

$$h_{ii,t+f} = \sum_{j=0}^{f-1} \omega_i (\alpha_i + \beta_i)^j + (\alpha_i + \beta_i)^f h_{ii,t}, \tag{20}$$

where $\omega_i, \alpha_i, \beta_i$ are the estimated GARCH parameters.

The conditional correlation matrix $\mathbf{R}$ is assumed to be constant over time calculated through the standardised residuals, which are defined as:

$$z_{i,t} = \frac{e_{i,t}}{\sqrt{h_{ii,t}}}, \tag{21}$$

where $e_{i,t}$ are the residuals of the return series, which are used to estimate the conditional correla-

tion matrix.

2.3.2 Dynamic Conditional Correlations (DCC)

The DCC model of Engle (2002) extends the CCC model by allowing correlations to vary over time while retaining the GARCH framework for variances. This is achieved by replacing the constant correlation matrix in Eq. (19) with a dynamic correlation matrix $\mathbf{R}_t$.

To accommodate multi-step forecasting for practical portfolio management, we follow the methodology of Engle and Sheppard (2001). The F-step ahead conditional covariance forecast is:

$$\widehat{\boldsymbol{\Sigma}}_{t+1:t+F} = \frac{1}{F} \sum_{f=1}^{F} \mathbf{D}_{t+f} \mathbf{R}_{t+f} \mathbf{D}_{t+f}, \tag{22}$$

where $\mathbf{D}_{t+f}$ is defined as in Eq. (19), and $\mathbf{R}_{t+f}$ is the f-step ahead forecast of the dynamic conditional correlation matrix. The multi-step forecast for the correlation matrix is computed as follows:

$$\mathbf{R}_{t+f} = \sum_{j=0}^{f-1} (1 - \alpha - \beta)\overline{\mathbf{Q}}(\alpha + \beta)^j + (\alpha + \beta)^f \mathbf{R}_t, \tag{23}$$

where $\overline{\mathbf{Q}}$ is the unconditional correlation matrix, and $\alpha + \beta < 1$ ensures stationarity. The parameters α and β control the persistence of the dynamic correlations.

The conditional correlation matrix $\mathbf{R}_t$ evolves over time according to:

$$\mathbf{R}_t = \mathbf{V}_t^{-1} \mathbf{Q}_t \mathbf{V}_t^{-1} \tag{24}$$

$$\mathbf{Q}_t = (1 - \alpha - \beta)\overline{\mathbf{Q}} + \alpha \mathbf{z}_{t-1} \mathbf{z}_{t-1}' + \beta \mathbf{Q}_{t-1}, \tag{25}$$

where $\mathbf{V}_t = \text{diag}\{\sqrt{q_{11,t}}, \sqrt{q_{22,t}}, \ldots, \sqrt{q_{NN,t}}\}$ ensures that $\mathbf{R}_t$ remains a proper correlation matrix. The standardised residuals $\mathbf{z}_t$ are defined as in Eq. (21), and $\overline{\mathbf{Q}}$ is estimated from historical standardised residuals.

2.3.3 Nonlinear Shrinkage Dynamic Conditional Correlations (DCC^{NL})

One work that combines the multivariate GARCH with a nonlinear shrinkage is the model of Engle et al. (2019). The covariance forecast in the DCC^{NL} model follows the same structure as in

Eq. (22), but now with a shrinkage-improved correlation matrix ($\overline{\mathbf{Q}}$). The original model uses the numerical method of Ledoit and Wolf (2015). However, we apply the nonlinear shrinkage method of Ledoit and Wolf (2020) to speed up the computations, which optimally shrinks the eigenvalues of the sample covariance matrix towards a better-conditioned target matrix.

Given a sample correlation matrix $\mathbf{\Upsilon}$, the optimal nonlinear shrinkage estimator adjusts its eigenvalues as follows. Let $\mathbf{\Upsilon}$ have the eigendecomposition:

$$\mathbf{\Upsilon} = \mathbf{U}\mathbf{\Lambda}\mathbf{U}^{\top}, \tag{26}$$

The nonlinear shrinkage transformation replaces $\mathbf{\Lambda}$ with a shrinkage-transformed version $\mathbf{\Lambda}^{*}$:

$$\mathbf{\Upsilon}^{*} = \mathbf{U}\mathbf{\Lambda}^{*}\mathbf{U}^{\top} \tag{27}$$

where the optimally shrunk eigenvalues λ_i^{*} are computed using the oracle nonlinear shrinkage function:

$$\lambda_i^{*} = \lambda_i \frac{1}{\left(\pi c \lambda_i f(\lambda_i)\right)^2 + \left(1 - c - \pi c \lambda_i H_f(\lambda_i)\right)^2} \tag{28}$$

where $f(\lambda_i)$ is the sample spectral density estimator, $H_f(\lambda_i)$ is the Hilbert transform of the spectral density, and $c = \frac{N}{T}$ is the limiting concentration ratio of the covariance matrix.

The sample spectral density function $f(x)$ is estimated using a kernel-based density estimator, ensuring uniform consistency. The Hilbert transform $H_f(x)$ is computed using the principal value integral, which corrects for eigenvalue bias induced by sampling variability.

The shrunk correlation matrix ($\mathbf{\Upsilon}^{*}$) is then used as the input for the DCC process in Eq. (24).

2.4 CNN with A-BiLSTM (CAB)

In our proposed model, each batch of input data is processed sequentially through all six stages, as described below.

2.4.1 Data Preprocessing

Let $\mathbf{B} = [\mathbf{D}_1, \mathbf{D}_2, \ldots, \mathbf{D}_T]^{\top}$ be the time series data, where each $\mathbf{D}_t \in \mathbb{R}^{N \times N}$ represents the rolling covariance matrix, normalised, of N assets at time t).

It is essential to standardise the input features to facilitate efficient training and convergence of

the CAB model. This transformation ensures that each feature has zero mean and unit variance, which is crucial for stabilising the training dynamics of neural networks.

We transform the data into overlapping sequences using a rolling window approach to capture temporal dependencies. Specifically, for a given lookback period L, the sequence creation process, at time t, can be expressed as:

$$\mathbf{S}_t = [\mathbf{D}_{t-L}, \mathbf{D}_{t-L+1}, \ldots, \mathbf{D}_t]^\top \in \mathbb{R}^{L \times N \times N} \tag{29}$$

The input to the CAB model consists of sequences of scaled covariance matrices. Formally, let $\mathbf{S}_i \in \mathbb{R}^{L \times N \times N}$ denote the i-th sequence.

2.4.2 3D Convolutional Layer

Next, each sequence of covariance matrices is processed through a three-dimensional layer (Lecun et al., 1998). We use a 3D CNN to capture local spatio-temporal features, given that each rolling covariance matrix is an $(N \times N)$ grid, and the temporal dimension arises from stacking these grids over time. The 3D CNN filters can identify how subsets of assets interact and evolve over multiple past windows, offering a more flexible approach than linear assumptions.

By applying a convolution operation with a kernel size of $(ks \times ks \times ks)$, the same padding, and a stride equal to one, the CNN layer captures patterns within the data across different time steps and different dimensions of the covariance matrices. The transformation performed by the 3D convolutional layer on the input sequence of covariance matrices can be expressed as:

$$\mathbf{X}_{\text{conv}}(t, i, j) = \sum_{u=-\lfloor ks/2 \rfloor}^{\lfloor ks/2 \rfloor} \sum_{v=-\lfloor k_s/2 \rfloor}^{\lfloor ks/2 \rfloor} \sum_{w=-\lfloor ks/2 \rfloor}^{\lfloor ks/2 \rfloor} \mathbf{W}(u, v, w) \cdot \mathbf{X}_{\text{rs}}(t + u, i + v, j + w) + b \tag{30}$$

where ks is the kernel size of the 3D Convolution, determining the dimensions of the receptive field across the temporal and spatial axes. $\mathbf{W}(u, v, w)$ represents the kernel weights, a learnable parameter of size $C_{\text{out}} \times C_{\text{in}} \times k_s \times k_s \times k_s$, where C_{in} is the number of input channels, and C_{out} is the number of output channels. The input covariance matrices are reshaped to include a single channel, so $C_{\text{in}} = 1$. Additionally, the model outputs a single channel, meaning $C_{\text{out}} = 1$. Consequently, the weight tensor simplifies to $\mathbf{W} \in \mathbb{R}^{1 \times 1 \times ks \times ks \times ks}$. $\mathbf{X}_{\text{rs}}(t + u, i + v, j + w)$ is the input sequence

of covariance matrices reshaped to dimensions $1 \times L \times N \times N$. The term b denotes the bias added to the convolution result, which, with $C_{\text{out}} = 1$, is a single scalar, i.e., $b \in \mathbb{R}^1$. The indices u, v, and w iterate over all whole integers within the range $[-(k_s/2), (k_s/2)]$, centered around (t, i, j), to compute local features. Finally, zero-padding is applied to ensure that the output dimensions match the input dimensions, preserving the temporal and spatial resolution of the covariance matrices.

Subsequently, the convolutional output is flattened ($\mathbf{X}_{\text{flattened}} \in \mathbb{R}^{L \times N^2}$) to transition from spatial to feature dimensions suitable for the LSTM layer. This reshaping consolidates the $N \times N$ covariance matrices into N^2-dimensional feature vectors for each time step within the sequence.

2.4.3   Bidirectional LSTM (BiLSTM) Layer

Following the CNN, the flattened transformed sequences are fed into a layer configured with u layers and h_d hidden dimension. To understand the BiLSTM, it is essential first to grasp the fundamentals of a standard LSTM network (Hochreiter, 1997). Appendix A.1 provides more detailed information on how each LSTM cell works.

The BiLSTM enhances the standard LSTM by adding another layer that processes the input sequence in the reverse order. This bidirectional approach allows the model to have both forward and backward information about the sequence, making it more effective in capturing the context from past and future data points. Each sequence goes through u layers, i.e. the output of layer one serves as input for layer 2.

In our model, the BiLSTM first transforms the input sequence $\mathbf{X}_{\text{flattened}}$ of dimension $L \times N^2$ into an output sequence of dimension $L \times 2h_d$. The BiLSTM uses learnable parameters to map the N^2 features at each time step into a lower-dimensional hidden representation of size h_d. This transformation is achieved through linear transformations, where weights and biases are optimised during training. Then, the hidden states from both forward and backward pass across all layers, and time steps are concatenated to form a comprehensive hidden state matrix. This matrix captures information from all directions and spans the entire sequence of inputs. Each BiLSTM layer can be expressed as:

$$\mathbf{H}^o = \left[\mathbf{H}^{(1)}, \mathbf{H}^{(2)}, \ldots, \mathbf{H}^{(h_d)} \right] \in \mathbb{R}^{L \times 2h_d} \tag{31}$$

where o represents the BiLSTM layer, for $o = 1, \ldots, u$, and each $\mathbf{H}^{(l)}$ for $l = 1, 2, \ldots, h_d$ is defined as:

14

$$\mathbf{H}^{(l)} = \begin{bmatrix} \overrightarrow{\mathbf{h}}_{t-L}^{(l)} & \overleftarrow{\mathbf{h}}_{t-L}^{(l)} \\ \overrightarrow{\mathbf{h}}_{t-L+1}^{(l)} & \overleftarrow{\mathbf{h}}_{t-L+1}^{(l)} \\ \vdots & \vdots \\ \overrightarrow{\mathbf{h}}_{t}^{(l)} & \overleftarrow{\mathbf{h}}_{t}^{(l)} \end{bmatrix} \in \mathbb{R}^{L \times 2} \tag{32}$$

The hidden dimension for each LSTM direction, denoted as h_d, results in a concatenated hidden state dimension of $2h_d$ at each time step.

The traditional BiLSTM outputs the last time step of the last layer. However, in our model, we use a similar approach to Liu and Guo (2019) methodology, meaning all time steps from the last layer ($\mathbf{H}^u$) are used as an input to our following steps. This procedure allows the attention mechanism to dynamically weigh the importance of each time step, enabling the model to focus on the most relevant temporal patterns when making predictions. By leveraging all time steps from the last layer ($\mathbf{H}^u$), rather than just the final output, the model can more effectively capture long-term dependencies and contextual relationships.

To mitigate overfitting and enhance the model's generalisation capabilities, a Dropout Layer is applied to the BiLSTM output. This operation randomly zeroes a fraction of the elements in $\mathbf{H}^u$ with a probability of 20%, effectively regularising the model by preventing reliance on specific neurons during training. During our testing phase, this feature will be skipped.

2.4.4 Multi-Head Self-Attention Layer

Our next step is to apply a multi-head attention mechanism (Vaswani et al., 2017) to each hidden state of the last layer. The multi-head attention mechanism to refine the temporal dependencies captured in the sequence. For h_e attention heads, the input $\mathbf{H}^u$ is used to compute the queries ($\mathbf{Q}$), keys ($\mathbf{K}$), and values ($\mathbf{V}$): $\mathbf{Q} = \mathbf{H}^u\mathbf{W}_q$, $\mathbf{K} = \mathbf{H}^u\mathbf{W}_k$, and $\mathbf{V} = \mathbf{H}^u\mathbf{W}_v$, where $\mathbf{W}_q, \mathbf{W}_k, \mathbf{W}_v \in \mathbb{R}^{2h_d \times 2h_d}$ are learnable parameters. The attention weights for each head are computed as follows:

$$\mathbf{Attention}(\mathbf{Q}_{\text{head}}, \mathbf{K}_{\text{head}}, \mathbf{V}_{\text{head}}) = \text{softmax}\left(\frac{\mathbf{Q}_{\text{head}}\mathbf{K}_{\text{head}}^{\top}}{\sqrt{d_k}}\right)\mathbf{V}_{\text{head}} \in \mathbb{R}^{L \times d_k} \tag{33}$$

where $d_k = \frac{2h_d}{h_e}$ scales the dot product to stabilise gradients and splits the features. Each head processes its respective portion of the features, which are concatenated to produce $\mathbf{A}_{concat} \in \mathbb{R}^{L \times 2h_d}$. The concatenated output is projected back to $\mathbf{A} = \mathbf{A}_{concat}\mathbf{W}_c \in \mathbb{R}^{L \times 2h_d}$ using a linear transforma-

tion.

The attention output is mean-pooled along the sequence dimension to condense the temporal information into a fixed-length representation:

$$\mathbf{a}_{\text{mean}} = \frac{1}{L} \sum_{t=1}^{L} \mathbf{A}_t \quad \in \mathbb{R}^{1 \times 2h_d} \tag{34}$$

where $\mathbf{A}_t$ is the t-th row of $\mathbf{A}$. This averaged context vector $\mathbf{a}_{\text{mean}}$ encapsulates the overall information from the entire sequence. We then pass $\mathbf{a}_{\text{mean}}$ through a fully connected layer to map it back to the covariance matrix space:

This averaged context vector $\mathbf{a}_{\text{mean}}$ encapsulates the overall information from the entire sequence. We then pass $\mathbf{a}_{\text{mean}}$ through a fully connected layer to map it back to the covariance matrix space:

$$\mathbf{y} = \mathbf{a}_{\text{mean}} \mathbf{W}_{\text{fc}} + \mathbf{b}_{\text{fc}} \quad \in \mathbb{R}^{1 \times N^2} \tag{35}$$

where $\mathbf{W}_{\text{fc}}$ and $\mathbf{b}_{\text{fc}}$ are receptively the weight matrix and bias vector of the fully connected layer.

Because our pipeline stacks 3D Convolution, BiLSTM, and attention in succession, the final latent representation becomes highly abstract, making interpretability at each layer difficult. Consequently, we do not attempt to interpret the hidden states or attention weights in a domain sense.

2.4.5 Enforcing Symmetry and Positive Semi-Definiteness

The output vector $\mathbf{y}$ is reshaped into a square matrix ($\mathbf{Y}_{\text{reshaped}} \in \mathbb{R}^{N \times N}$) to form the predicted covariance matrix.

The output matrix $\mathbf{Y}_{\text{reshaped}}$ may not necessarily be symmetric, a key property of covariance matrices. To enforce symmetry, we average the matrix with its transpose:

$$\mathbf{Y}_{\text{sym}} = \frac{\mathbf{Y}_{\text{reshaped}} + \mathbf{Y}_{\text{reshaped}}^{\top}}{2} \tag{36}$$

Then, we rescale the normalised output back to the original scale of the data, using the reverse process of Section 2.4.1 resulting in $\mathbf{Y}_{\text{sym}}^{unscaled}$.

Symmetry alone does not guarantee that $\mathbf{Y}_{\text{sym}}^{unscaled}$ is positive semi-definite, which is another requisite property of covariance matrices. To ensure positive semi-definiteness, we perform eigen-

value decomposition:

$$\mathbf{Y}_{\text{sym}}^{unscaled} = \mathbf{U}\mathbf{\Lambda}\mathbf{U}^\top \tag{37}$$

We then modify $\mathbf{\Lambda}$ by setting all negative eigenvalues to zero:

$$\mathbf{\Lambda}' = \text{diag}\left(\max(\lambda_i, 0)\right) \tag{38}$$

The positive semi-definite matrix is reconstructed as:

$$\mathbf{Y}_{\text{psd}} = \mathbf{U}\mathbf{\Lambda}'\mathbf{U}^\top \tag{39}$$

2.4.6 Shrinkage

While DL-based forecasts can learn intricate patterns, which provide a more stable forecast, the noisy historical covariance may still convey valuable information about recent market conditions. Therefore, our model's final step is incorporating a linear shrinkage from historical values in our predictions.

$$\mathbf{CAB} = \mathbf{Y}_{\text{psd}}\dot{\phi} + \mathbf{\Sigma}_{t-F:t}\dot{(1-\phi)} \tag{40}$$

where $\mathbf{CAB}$ is the final $N \times N$ matrix output, and ϕ is the shrinkage factor.

2.5 Evaluation metrics

We will use performance metrics consistent with previous literature (Symitsi et al., 2018; Bollerslev et al., 2018; Zhang et al., 2024) to check the models' performance. We consider the following loss functions to measure the average distance between predicted covariances and realised covariances matrices for the model comparisons:

$$\mathcal{L}_t^E = \sqrt{\text{vec}_{Tri}(\mathbf{\Sigma}_t - \hat{\mathbf{\Sigma}}_t)^\top \, \text{vec}_{Tri}\left(\mathbf{\Sigma}_t - \hat{\mathbf{\Sigma}}_t\right)} \tag{41}$$

$$\mathcal{L}_t^F = \sqrt{\text{Tr}\left[\left(\mathbf{\Sigma}_t - \hat{\mathbf{\Sigma}}_t\right)^\top \left(\mathbf{\Sigma}_t - \hat{\mathbf{\Sigma}}_t\right)\right]} \tag{42}$$

where $\mathcal{L}_t^E$ represents the Euclidean distance between the $N(N+1)/2$ dimensional vectorised version of the upper triangular of forecast covariances and ex-post realised covariances. $\mathcal{L}_t^F$ is the

Frobenius distance between the two matrices, and Tr is the trace of a square matrix. All these functions measure losses. Therefore, lower values are preferred.

3 Empirical Results

We obtain our sample data from the Refinitiv Database, covering daily adjusted closing prices of 14 major ETFs that reflect equity and bond markets across diverse global sectors. These ETFs were selected to construct a multi-asset environment that includes equity sectors (e.g. technology, financials, industrials, consumer staples) and fixed-income exposures. Table 1 details the ETF's information. To compute *excess* returns, we also retrieve from the Federal Reserve Economic Data the 1-month U.S. Treasury yield, treating it as a daily risk-free rate. Our sample runs from 1 January 2017 to 31 December 2023, totalling 1,760 trading days.

Table 1 – List of ETFs included in our research.

Name	Ticker	ISIN	Asset Class
iShares Global Tech ETF	IXN	US4642872919	Equity
iShares Global Financials ETF	IXG	US4642873339	Equity
iShares Global Consumer Discretionary ETF	RXI	US4642887453	Equity
iShares Global Industrials ETF	EXI	US4642887297	Equity
iShares Global Healthcare ETF	IXJ	US4642873255	Equity
iShares Global Consumer Staples ETF	KXI	US4642887370	Equity
iShares U.S. Real Estate ETF	IYR	US4642877397	Real Estate
iShares International Developed Real Estate ETF	IFGL	US4642884898	Real Estate
iShares Global Materials ETF	MXI	US4642886950	Equity
iShares Global Energy ETF	IXC	US4642873412	Equity
iShares Global Comm Services ETF	IXP	US4642872752	Equity
iShares Global Utilities ETF	JXI	US4642887115	Equity
iShares Core U.S. Aggregate Bond ETF	AGG	US4642872265	Fixed Income
iShares Core International Aggregate Bond ETF	IAGG	US46435G6724	Fixed Income

We split our dataset into a training period from 1 January 2017 to 31 December 2020 and a testing period covering 1 January 2021 to 31 December 2023. The testing sample thus comprises 753 trading days, encompassing a wide range of economic and market conditions. We identify three distinct market regimes within this testing window to examine whether our model responds robustly to varying interest-rate and equity-market environments. We designate the interval be-

tween 1 January 2021 and 2 January 2022 as the *First Bull Period* (Bull-1), typified by low yields on the risk-free asset and a generally stable equity market. We label the interval from 3 January 2022 to 12 June 2022 as the *Bear Period* (Bear), characterised by a steady rise in the risk-free rate and a drop of 20% or more in the S&P 500 from its last peak. Lastly, we classify the interval from 13 June 2022 to 31 December 2023 as the *Second Bull Period* (Bull-2), featuring persistently high interest rates but a renewed upswing in equity prices. This subdivision ensures that our out-of-sample evaluations capture both low- and high-rate market phases and a bear-market regime, offering a comprehensive test of the model's ability to adapt to evolving financial landscapes.

During the training period, we minimise the Frobenius distance (Eq. 42) to select hyperparameters. We use *Optuna* (Akiba et al., 2019) for hyperparameter selection. Appendix A.2 shows the grid search table. Specifically, we split the training dataset into a model-fitting subset (80%) and a validation subset (20%) to identify optimal settings under a forecast horizon (F) of 20 days. We adopt the Adam optimiser over 100 epochs, using a batch size of 128 and a learning rate of 10^{-4}. For the neural-network-based CAB model, we use a lookback window (L) of 100 days. We set the 3D convolution kernel size (ks) to five; the BiLSTM has 128 hidden dimensions (hd) across seven stacked layers (u), and the multi-head attention uses 16 heads (he). Finally, we apply a shrinkage factor of 0.8 (ϕ) when combining the DL output with the most recent historical covariance.

We conduct a rolling forecast procedure to simulate live conditions. Each new trading day t in the test set triggers an online update of our DL model, incorporating all data up through day t. This design ensures the forecasts mimic a real-world trading environment, where only up-to-date historical data is available at each decision point.

Table 2 reports the average Euclidean ($\mathcal{L}^E$) and Frobenius ($\mathcal{L}^F$) distances between forecasted and realised covariance matrices for all models over the entire testing period (2021–2023)[4]. GARCH models (CCC and DCC) and $EWMA$ perform relatively well as they adapt faster to structural changes in the covariance matrices. Please note that although DCC^{NL} is not more accurate than the traditional DCC, it provides more stable forecasts based on the eigenvalues. However, our model (CAB) yields the lowest errors in both metrics, outperforming classical benchmarks. Dimensional reduction models perform inadequately as we only use 14 assets.

---

[4]Bold and underlined numbers represent the lowest and the second lowest values, respectively.

Table 2 – Average Euclidean ($\mathcal{L}^E$) and Frobenius ($\mathcal{L}^F$) distances ($\times 10^5$) for whole the testing period (1 January 2021 to 31 December 2023).

	$\mathcal{L}^E$	$\mathcal{L}^F$
NA	53.526	82.020
NA^F	52.713	80.987
$EWMA$	49.111	75.349
PCA	54.348	83.154
RMT	54.145	82.915
LW	49.772	76.514
LW^F	68.136	103.363
CCC	48.568	75.198
DCC	<u>48.268</u>	<u>74.716</u>
DCC^{NL}	51.621	79.079
CAB	**38.312**	**58.923**

To solidify our findings, we analysed the 10 models with 753 paired samples for the Euclidean and Frobenius distances following Demsar (2006) frequentist methodology. The significance level is $\alpha = 0.050$ for all tests here forward. We rejected the null hypothesis that the population is normal for all the populations ($p < 0.01$ for all models in both distances). Therefore, we assume that not all populations are normal.

Because we have more than two populations and the populations are not normal, we use the non-parametric Friedman test as an omnibus test to determine if there are any significant differences between the median values of the populations. We use the post-hoc Nemenyi test to infer which differences are significant. Differences between populations are significant if the difference in the mean rank is greater than the critical distance CD=0.494 of the Nemenyi test.

We reject the Friedman test's null hypothesis, which states that there is no difference in the central tendency of the populations. Therefore, we assume that there is a statistically significant difference between the central tendencies of the populations. Figure 1 shows the post-hoc Nemenyi test critical distance between groups. Our model reports statistically better results than the benchmark models.

Table 3 presents the average distance metrics for the testing period across three market regimes: Bull-1, Bear, and Bull-2. Overall, the CAB model consistently outperforms all benchmarks.

While all models experience a decrease in accuracy during the turbulent Bear regime, the CAB

(a) Upper Triangular Euclidean distance
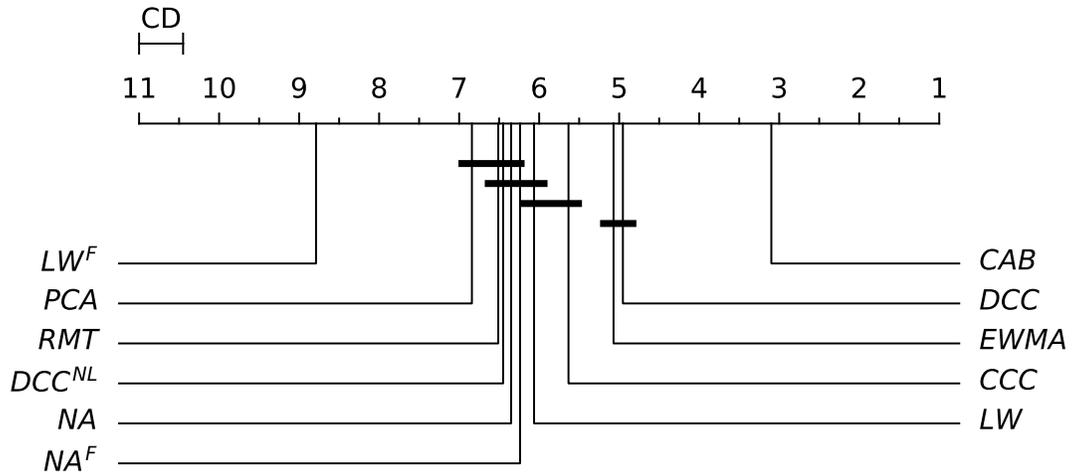
(b) Frobenius distance
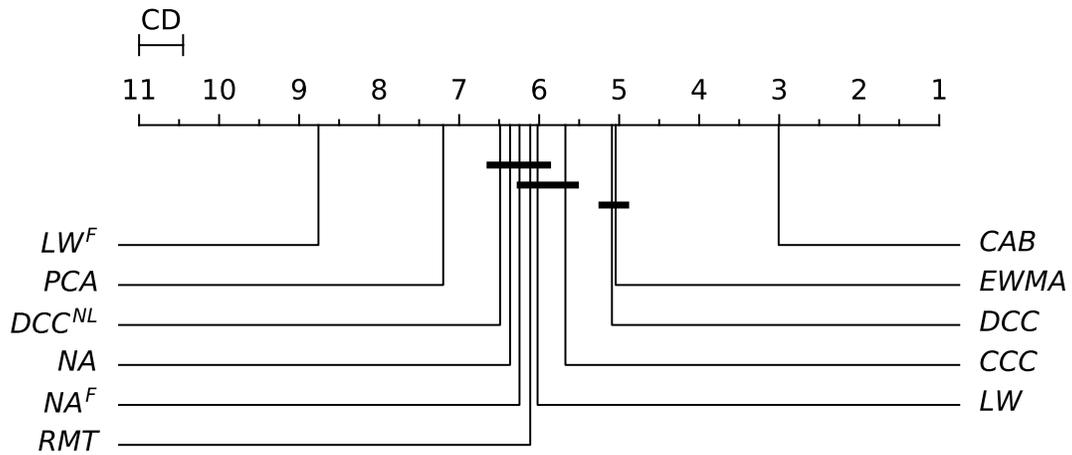
Figure 1 – Critical distance diagrams for the post-hoc Nemenyi test.

Table 3 – Average Euclidean ($\mathcal{L}^E$) and Frobenius ($\mathcal{L}^F$) distances ($\times 10^5$) for different testing periods: Bull-1 (1 January 2021 to 2 January 2022), Bear (3 January 2022 to 12 June 2022), and Bull-2 (13 June 2022 to 31 December 2023).

	Bull-1		Bear		Bull-2	
	$\mathcal{L}^E$	$\mathcal{L}^F$	$\mathcal{L}^E$	$\mathcal{L}^F$	$\mathcal{L}^E$	$\mathcal{L}^F$
NA	36.937	56.621	89.891	137.868	53.709	82.252
NA^F	35.680	54.992	98.002	150.780	50.586	77.545
$EWMA$	31.754	<u>48.973</u>	<u>82.799</u>	<u>126.614</u>	50.574	77.549
PCA	37.424	57.281	90.720	139.116	54.747	83.660
RMT	37.246	57.083	90.638	138.821	54.493	83.411
LW	34.126	52.599	90.441	138.173	48.089	74.088
LW^F	63.288	94.759	93.189	143.636	63.989	97.222
CCC	<u>31.688</u>	49.784	88.106	134.902	48.017	74.316
DCC	33.516	52.166	84.745	130.345	<u>47.227</u>	<u>73.161</u>
DCC^{NL}	36.779	56.449	87.650	134.167	50.767	77.734
CAB	**24.276**	**37.643**	**66.381**	**102.252**	**39.253**	**60.126**

approach exhibits notable robustness. In particular, during the Bull-2 period, characterised by elevated interest rates and dynamic shifts in cross-asset relationships, integrating DL techniques with classical shrinkage enables CAB to adapt effectively to changing market conditions, thereby maintaining lower distance metrics.

Supplementary Nemenyi post-hoc tests confirm that the performance improvements observed with CAB are statistically significant. These tests provide further evidence that the model's superior performance is not merely a result of sample-specific idiosyncrasies but reflects a robust ability to handle varying market regimes.

Moreover, these findings contribute to the literature on hybrid forecasting methods by demonstrating that blending modern DL with traditional econometric techniques can offer substantial gains in predictive accuracy, especially in periods of market stress. This robust performance under diverse macroeconomic conditions highlights the practical relevance of the CAB approach for risk management and strategic asset allocation.

4   Robustness analysis

4.1   Larger dataset

In this section, we expand our asset universe to 260 ETFs to evaluate whether our model continues to outperform established benchmarks in a high-dimensional setting. Appendix A2 provides a comprehensive list of the ETFs in a multi-asset portfolio. Table 4 presents the corresponding performance metrics.

Table 4 – Average Euclidean ($\mathcal{L}^E$) and Frobenius ($\mathcal{L}^F$) distances ($\times 10^3$) using 260 ETFs for $F = 20$ and *excess* returns for different testing periods: Overall (1 January 2021 to 31 December 2023), Bull-1 (1 January 2021 to 2 January 2022), Bear (3 January 2022 to 12 June 2022), and Bull-2 (13 June 2022 to 31 December 2023).

	Overall		Bull-1		Bear		Bull-2	
	$\mathcal{L}^E$	$\mathcal{L}^F$	$\mathcal{L}^E$	$\mathcal{L}^F$	$\mathcal{L}^E$	$\mathcal{L}^F$	$\mathcal{L}^E$	$\mathcal{L}^F$
NA	11.546	16.484	8.677	12.442	20.458	29.257	10.814	15.390
NA^F	10.792	15.399	7.661	11.014	20.742	29.532	9.927	14.130
$EWMA$	10.544	15.054	7.518	10.802	18.410	26.292	10.219	14.543
LW	10.719	15.304	8.095	11.619	19.933	28.458	9.740	13.867
LW^F	13.460	19.170	12.098	17.270	19.374	27.609	12.622	17.947
CCC	<u>10.260</u>	<u>14.647</u>	<u>7.368</u>	<u>10.587</u>	18.723	26.687	9.674	13.777
DCC	10.280	14.671	7.796	11.182	<u>18.076</u>	<u>25.777</u>	<u>9.622</u>	<u>13.703</u>
DCC^{NL}	11.047	15.747	8.597	12.301	18.687	26.634	10.414	14.814
PCA	11.658	16.643	8.743	12.535	20.625	29.500	10.939	15.567
RMT	11.652	16.636	8.738	12.529	20.618	29.490	10.934	15.561
CAB	**8.933**	**12.789**	**5.447**	**7.893**	**15.722**	**22.456**	**9.220**	**13.153**

Our proposed approach (CAB) consistently outperforms the benchmark models, reflected by its lower average Euclidean and Frobenius distances across most periods. Notably, during the Overall, Bull-1, and Bull-2 periods, the post-hoc Nemenyi test confirms that the outperformance of CAB is statistically significant. In contrast, during the Bear period, CAB's performance is statistically similar to that of the DCC and $EWMA$ models.

4.2 Impact of Using Raw Returns vs. Excess Returns

One potential criticism of our model is that it may be overly tailored to *excess* returns, even though some classic optimisation frameworks (Markowitz, 1952) often use *raw* returns. We re-estimate our model without subtracting the risk-free rate to address this concern. All other model parameters remain identical to those described in Section 2, with the sole difference being that $\mathbf{r}_t$ now represents the N-dimensional row vector of *raw* daily returns for N assets at time t.

Table 5 reports the performance of the various models under these *raw* returns assumptions. Our approach (CAB) continues outperforming all benchmarks across the entire sample and within individual market regimes, with statistically significant results based on the same post-hoc Nemenyi criteria used earlier. This finding directly informs our second research question about whether *raw* vs. *excess* returns lead to materially different covariance forecasts. When comparing Table 5 (*raw* returns) to Tables 2 and 3 (*excess* returns), the numerical magnitudes change slightly, but the rank order remains the same: CAB still produces the most accurate forecasts overall.

Table 5 – Average Euclidean ($\mathcal{L}^E$) and Frobenius ($\mathcal{L}^F$) distances ($\times 10^5$) using *raw* returns for different testing periods: Overall (1 January 2021 to 31 December 2023), Bull-1 (1 January 2021 to 2 January 2022), Bear (3 January 2022 to 12 June 2022), and Bull-2 (13 June 2022 to 31 December 2023).

	Overall		Bull-1		Bear		Bull-2	
	$\mathcal{L}^E$	$\mathcal{L}^F$	$\mathcal{L}^E$	$\mathcal{L}^F$	$\mathcal{L}^E$	$\mathcal{L}^F$	$\mathcal{L}^E$	$\mathcal{L}^F$
NA	53.525	82.020	36.936	56.620	89.895	137.875	53.707	82.249
NA^F	52.486	80.668	34.913	53.883	98.623	151.717	50.462	77.372
$EWMA$	49.174	75.441	31.753	<u>48.972</u>	<u>82.798</u>	<u>126.613</u>	50.697	77.730
PCA	54.348	83.153	37.423	57.280	90.724	139.123	54.745	83.657
RMT	54.144	82.914	37.245	57.081	90.643	138.829	54.491	83.408
LW	49.771	76.512	34.125	52.598	90.442	138.174	48.087	74.085
LW^F	68.130	103.353	63.273	94.736	93.190	143.636	63.985	97.217
CCC	48.508	75.106	<u>31.599</u>	49.634	88.139	135.038	47.948	74.196
DCC	<u>48.232</u>	<u>74.661</u>	33.445	52.045	84.884	130.630	<u>47.161</u>	<u>73.050</u>
DCC^{NL}	51.604	79.051	36.691	56.305	87.856	134.535	50.731	77.664
CAB	**36.663**	**56.518**	**22.807**	**35.673**	**62.036**	**96.406**	**38.273**	**58.441**

Our findings indicate that the advantage of our framework is not contingent on the choice between *excess* or *raw* returns, reaffirming its robustness to the presence or absence of the risk-free

rate. Moreover, this consistency suggests that subtracting the risk-free rate over the medium-term horizon does not significantly alter the core structure of asset co-movements. Hence, even though economic theory posits that *excess* returns better capture risk premiums, our empirical results show that the forecasting edge of CAB holds across both *raw* and *excess* return specifications. In other words, our method retains its superior performance even when modelling raw returns, suggesting that its effectiveness does not hinge on subtracting the risk-free rate.

4.3 Varying Forecast Horizons

We also examine our model's behaviour as the forecast horizon (F) varies. In the baseline analysis, $F = 20$ days are medium-term, but many institutional investors face different time horizons for risk management or asset allocation decisions. In line with our first research question regarding under-explored medium-term horizons, we extend F from 10 to 250 days, thus covering short, medium, and long horizons. To explore model performance across this range of settings, we evaluate both *excess* (Table A3) and *raw* returns (Table A4).

Table A3 shows that our model consistently achieves the lowest average distance metrics across most forecast horizons. CAB remains among the top performers for shorter horizons ($F = 10$). However, it does not outperform GARCH-based models (CCC and DCC) and $EWMA$. These differences are not statistically different in the overall period, Bull-1 and Bull-2. During Bull-2, our model outperformed the benchmarks, and the results were statistically significant based on the post-hoc Nemenyi test.

For mid-term forecasting ($F = 40, 60, 90, 120, 180$) for both distances, the differences are statistically significant in all periods. Thus, our model consistently outperforms the benchmarks. Please note that GARCH models tend to underperform as the forecast horizon increases, while full data models (NA^F and LW^F) tend to diminish forecasting errors. Please note, while the DCC^{NL} was more recently designed for high dimensional matrices, it provides more stable forecasts based on eigenvalues than the classical DCC.

At the longest horizon ($F = 250$), CAB again excels in most periods. Besides showing a large difference between distances during the Bear period and Bull-1, the post-hoc Nemenyi test shows no statistical difference between our model and NA^F and LW^F, respectively. These results suggest that more complex models capture slower-moving cross-asset dynamics effectively, while classical estimators remain competitive in certain regime-specific conditions. As anticipated, naive

25

and shrinkage methods perform relatively well at the longer horizon. These patterns reinforce our first research question's premise that medium-term horizons can benefit from sophisticated models and highlight instances where simpler approaches hold their own.

Turning to Table A4, we link our findings to the second research question: whether using *raw* or *excess* returns makes a systematic difference. Results show that the top-performing models remain consistent across all forecast horizons.

Once again, CAB tends to yield the strongest overall performance. Although it does not dominate at shorter horizons, it consistently ranks near the top, showing no statistical difference between our model and the top performers. All other differences are statistically significant. These results mirror the trends seen under *excess* returns, indicating that the performance edge of CAB does not hinge on subtracting the risk-free rate. Therefore, our DL approach remains robust even if practitioners opt for *raw* returns, common in certain classical optimisation frameworks. Our model performs better than the benchmarks for longer horizons ($F = 250$). However, the results are not statistically different from the second-performing models (NA^F and LW^F) for the Bull-1 and Bear periods, respectively.

These findings indicate that DL-based models can adapt effectively across different forecast windows. Across both dimensions, CAB shows a stable advantage, with only minor variations in extreme horizons.

5   Economic Value in Portfolio Management

Next, we investigate the economic importance of accurate covariance forecasts in a practical asset allocation framework. Specifically, we consider an investor allocating wealth among the ETFs specified in Section 3, subject to a no-short-selling constraint. Such a constraint is common among regulated institutional investors (e.g., pension funds, mutual funds) that may face limits on leverage or short positions. We adopt daily, weekly, and monthly rebalancing intervals (Symitsi et al., 2018).

At each rebalancing date, the investor solves the GMV problem:

$$\min_{\boldsymbol{w}_t} \quad \mathbf{w}_t^\top \widehat{\boldsymbol{\Sigma}}_t \, \mathbf{w}_t \quad \text{subject to} \quad \mathbf{1}^\top \mathbf{w}_t = 1, \quad w_{i,t} \geq 0, \tag{43}$$

where $\mathbf{w}_t$ is an $N \times 1$ vector of GMV portfolio weights, $\widehat{\boldsymbol{\Sigma}}_t$ is the $N \times N$ forecast covariance from each model, and $\mathbf{1}$ is an $N \times 1$ vector of ones. Excluding expected returns from the optimi-

sation allows us to isolate the impact of covariance forecasts (DeMiguel et al., 2009; Kourtis et al., 2012).

Using a rolling forecast window, we generate 11 portfolio strategies (one for each forecast model) plus an equally weighted ($1/N$) benchmark. After estimating $\widehat{\Sigma}_t$, we compute the GMV weights and hold them until the next rebalancing date. We then record the ex-post average portfolio return for each model (m) as:

$$\mathbf{r}_{t+1}^{(m)} = \frac{1}{P} \sum_{t=1}^{P} \mathbf{w}_t^{(m)\top} \mathbf{r}_{t+1}, \tag{44}$$

where $\mathbf{r}_t$ is an $N \times 1$ vector of realised asset returns, P is the total out-of-sample length, and $\mathbf{w}_t^{(m)}$ are the portfolio weights at the start of period t for model m.

We focus on two main metrics to compare forecast models: out-of-sample portfolio *variance* and *turnover*. The variance of daily returns by a portfolio constructed by model m is:

$$\sigma_m^2 = \frac{1}{P} \sum_{t=1}^{P} \left(r_t^{(m)} - \bar{r}^{(m)} \right)^2 \tag{45}$$

where $r_t^{(m)}$ is the ex-post return of model m in period t, $\bar{r}^{(m)}$ and P is its mean and number of observations over the out-of-sample window. Meanwhile, the average turnover reflects how often the portfolio adjusts its weights:

$$\text{TO}_m = \frac{1}{P-1} \sum_{t=1}^{P-1} \left\| \mathbf{w}_{t+1}^{(m)} - \mathbf{w}_{t+}^{(m)} \right\|_1, \tag{46}$$

where $\mathbf{w}_{t+}^{(m)}$ are the portfolio weights of model m immediately before rebalancing at $t + 1$, and $\|\cdot\|_1$ is the 1-norm. A higher turnover implies more frequent portfolio adjustments, potentially incurring greater trading costs (Kourtis, 2014).

We also include an equally weighted ($1/N$) portfolio, often cited for its simplicity and historically strong performance (DeMiguel et al., 2009). Although $1/N$ avoids estimation risk and typically maintains low turnover, it cannot adapt to shifting market correlations.

From Table 6, it is evident that the covariance forecasts provided by the CAB model strike a competitive balance between risk reduction and turnover across all rebalancing horizons. Across daily, weekly, and monthly rebalancing horizons, CAB slightly trails the top daily performer,

approaches the leading weekly method, and matches or surpasses most other approaches monthly, thus consistently ranking among the best-performing models. This robust performance does not come at the cost of excessive turnover, as CAB's turnover measures remain moderate compared to methods that may obtain marginally lower variances only at the expense of frequent portfolio rebalancing (e.g., NA, DCC, DCC^{NL}).

Table 6 – performance of the global minimum variance portfolios constructed using the covariance forecasts from the 11 models under consideration plus the equal-weighted portfolio. The portfolios are compared based on their annualised out-of-sample standard deviation (σ_m) and average out-of-sample turnover (TO_m), respectively. Results for three different rebalancing frequencies are presented.

	Daily		Weekly		Monthly	
	σ_m^2	TO_m	σ_m^2	TO_m	σ_m^2	TO_m
$1/N$	0.018132	0.005733	0.018115	0.002567	0.018060	0.001282
NA	**0.001991**	0.125568	0.002527	0.055395	0.002631	0.025707
NA^F	0.002451	**0.001445**	0.002453	**0.000653**	**0.002461**	**0.000369**
$EWMA$	0.002475	0.079388	0.002482	0.037928	0.002554	0.016088
PCA	0.002680	0.197322	0.002722	0.072903	0.002657	0.023108
RMT	0.002647	0.125512	0.002689	0.055954	0.002733	0.024767
LW	0.002655	0.098020	0.003373	0.047089	0.003598	0.022957
LW^F	0.002774	<u>0.001816</u>	0.002777	<u>0.000956</u>	0.002784	<u>0.000620</u>
CCC	0.002281	0.126519	0.002580	0.049839	0.002713	0.014816
DCC	0.002075	0.116446	**0.002388**	0.051710	<u>0.002524</u>	0.017159
DCC^{NL}	0.002048	0.129453	0.002448	0.056173	0.002618	0.023470
CAB	<u>0.002293</u>	0.078799	<u>0.002428</u>	0.048383	0.002579	0.023807

When compared to the $1/N$ benchmark, please note that all models present a statistically significant lower annual variance, based on the one-side F-Test of equalities of variance.

Table 7 – Performance of the GMV portfolios constructed using the covariance forecasts from the 11 models under consideration plus the equal-weighted portfolio for the different market regimes. The portfolios are compared based on their annualised out-of-sample standard deviation (σ_m) and average out-of-sample turnover (TO$_m$), respectively.

		Daily		Weekly		Monthly	
		σ_m^2	TO_m	σ_m^2	TO_m	σ_m^2	TO_m
Bull-1	$1/N$	0.009883	0.005169	0.009873	0.002335	0.009907	0.001103
	NA	0.000543	0.150112	0.000794	0.060372	0.000834	0.026885
	NA^F	0.000731	<u>0.001378</u>	0.000732	**0.000607**	0.000736	0.000327
	$EWMA$	0.000735	0.088541	0.000748	0.043884	0.000754	0.015613
	PCA	0.000850	0.236835	0.000827	0.090803	0.000795	0.020906
	RMT	0.000856	0.150601	0.000860	0.067402	0.000826	0.025859
	LW	0.001054	0.091979	0.001572	0.044883	0.001692	0.022283
	LW^F	0.000780	**0.001228**	0.000781	<u>0.000610</u>	0.000783	<u>0.000349</u>
	CCC	0.000620	0.119486	<u>0.000681</u>	0.053221	<u>0.000728</u>	0.013605
	DCC	<u>0.000529</u>	0.207262	0.000698	0.093558	0.000781	0.024324
	DCC^{NL}	**0.000522**	0.217432	0.000784	0.097809	0.000875	0.034673
	CAB	0.000634	0.086489	**0.000656**	0.055931	**0.000707**	0.023736
Bear	$1/N$	0.029939	0.007221	0.029940	0.003443	0.029793	0.001599
	NA	**0.002207**	0.092111	0.002682	0.032018	0.002959	0.018142
	NA^F	0.002891	**0.001650**	0.002892	**0.000935**	0.002906	**0.000436**
	$EWMA$	0.002908	0.079065	0.002843	0.036314	0.003120	0.019997
	PCA	0.002800	0.114256	0.002792	0.043637	0.002864	0.011111
	RMT	0.002983	0.094396	0.002896	0.037508	0.003153	0.023308
	LW	0.003118	0.095723	0.003970	0.041663	0.004754	0.021610
	LW^F	0.003196	<u>0.002035</u>	0.003197	<u>0.001043</u>	0.003201	<u>0.000570</u>
	CCC	0.002497	0.129487	<u>0.002646</u>	0.043843	**0.002590**	0.012451
	DCC	0.002355	0.067768	**0.002639**	0.015372	<u>0.002636</u>	0.005911
	DCC^{NL}	<u>0.002269</u>	0.083567	0.002652	0.024277	0.002730	0.010308
	CAB	0.002273	0.030506	0.002464	0.022686	0.002656	0.016836

		Daily		Weekly		Monthly	
		σ_m^2	TO_m	σ_m^2	TO_m	σ_m^2	TO_m
	$1/N$	0.019967	0.005666	0.019956	0.002382	0.019933	0.001334
	NA	**0.002823**	0.118997	0.003526	0.053457	0.003667	0.029686
	NA^F	0.003398	**0.001426**	0.003400	**0.000577**	0.003406	**0.000261**
	$EWMA$	0.003432	0.073812	0.003433	0.034460	0.003630	0.016887
	PCA	0.003793	0.194898	0.003678	0.063899	0.003597	0.024379
Bull-2	RMT	0.003668	0.118539	0.003720	0.055498	0.003762	0.029837
	LW	0.003512	0.102531	0.004274	0.048313	0.004245	0.020765
	LW^F	0.003874	<u>0.002113</u>	0.003879	<u>0.001123</u>	0.003889	<u>0.000788</u>
	CCC	0.003233	0.129874	0.003635	0.047812	0.003671	0.015276
	DCC	0.002947	0.071444	**0.003294**	0.026871	**0.003364**	0.009476
	DCC^{NL}	<u>0.002924</u>	0.085242	<u>0.003318</u>	0.034070	<u>0.003365</u>	0.012661
	CAB	0.003323	0.087821	0.003547	0.052596	0.003885	0.029487

Examining the same metrics across distinct market regimes (Table 7) reveals that CAB remains a robust contender under varying conditions: in Bull-1, it consistently competes for the lowest variance, even attaining the best performance in weekly and monthly rebalancing; in the Bear regime, CAB ranks near the top in daily and weekly horizons, balancing lower turnover against marginally higher volatility than a few dynamic methods; and while Bull-2 sees other estimators occasionally surpass CAB, it still demonstrates stable risk control with moderate trading activity, indicating that its effectiveness persists across both tranquil and turbulent market environments.

Comparisons to the $1/N$ benchmark further highlight the importance of adaptivity. While $1/N$ offers minimal turnover, it endures noticeably higher variance in all market conditions, reflecting its inability to exploit up-to-date correlation information. Indeed, the difference in annualised variances between CAB and $1/N$ can reach 80-90 basis points in certain scenarios, a gap that can substantially affect risk-adjusted returns and capital preservation.

Overall, CAB tends to exhibit moderate turnover, balancing the need to adjust to changing correlations without incurring unnecessary trades. This stability benefits investors who must limit transaction costs or adhere to regulatory constraints on turnover. These results underscore that advanced covariance forecast can yield *economically meaningful* improvements in risk control, particularly over the medium-term horizons favoured by many institutional investors. The CAB

model stands out by combining strong variance reduction with stable rebalancing behaviour, balancing responsiveness to market changes and turnover efficiency.

6   Conclusion

We propose a novel DL framework for medium-term covariance forecasting in multi-asset portfolios, combining 3D convolutions, bidirectional LSTMs, and multi-head attention. Empirical tests on various ETFs from 2017 to 2023 reveal that this model, enhanced by a final shrinkage step, consistently outperforms classical benchmarks across different forecast horizons and market regimes.

Notably, its performance advantage remains robust whether one subtracts a risk-free rate from returns, suggesting broad applicability in diverse portfolio management practices.

In portfolio experiments, the proposed method enables GMV strategies to achieve lower out-of-sample volatility with moderate turnover, underlining the tangible economic value of improved covariance forecast. By bridging cutting-edge DL techniques with established financial principles, our work highlights the promise of sophisticated spatiotemporal modelling for risk management and allocation decisions, especially at horizons where structural shifts and evolving correlations pose unique forecasting challenges.

Still, two research avenues warrant further exploration. First, extending the network architecture to accommodate skewed or heavy-tailed distributions could better capture tail risk in times of market stress. Second, explicitly incorporating transaction costs or liquidity constraints within the optimisation process might yield more realistic and implementable trading strategies.

We hope these findings encourage the finance community to explore and adapt advanced neural architectures for medium-term and long-horizon applications, strengthening the link between machine learning innovation and effective real-world asset allocation.

References

Akiba, T., Sano, S., Yanase, T., Ohta, T., and Koyama, M. (2019). Optuna: A next-generation hyperparameter optimization framework. In *Proceedings of the 25th ACM SIGKDD International Conference on Knowledge Discovery & Data Mining*, pages 2623–2631. ACM. 3

Baillie, R. T. and Bollerslev, T. (1992). Prediction in dynamic models with time-dependent conditional variances. *Journal of Econometrics*, 52(1):91–113. 2.3.1

Bollerslev, T. (1990). Modelling the coherence in short-run nominal exchange rates: A multivariate generalized arch model. *The Review of Economics and Statistics*, 72(3):498–505. 1, 2.3.1

Bollerslev, T., Patton, A. J., and Quaedvlieg, R. (2018). Modeling and forecasting (un)reliable realized covariances for more reliable financial decisions. *Journal of Econometrics*, 207(1):71–91. 1, 2.5

Chiriac, R. and Voev, V. (2011). Modelling and forecasting multivariate realized volatility. *Journal of Applied Econometrics*, 26(6):922–947. 1

Cont, R. (2001). Empirical properties of asset returns: stylized facts and statistical issues. *Quantitative Finance*, 1(2):223. 2

Corsi, F. (2009). A simple approximate long-memory model of realized volatility. *Journal of Financial Econometrics*, 7(2):174–196. 1

De Nard, G., Engle, R. F., Ledoit, O., and Wolf, M. (2022). Large dynamic covariance matrices: Enhancements based on intraday data. *Journal of Banking & Finance*, 138:106426. 1

De Nard, G., Ledoit, O., and Wolf, M. (2021). Factor models for portfolio selection in large dimensions: The good, the better and the ugly. *Journal of Financial Econometrics*, 19(2):236–257. 1, 2.3.1

De Nard, G., Ledoit, O., and Wolf, M. (2024). Improved tracking-error management for active and passive investing. *Available at SSRN 4898624*. 1

DeMiguel, V., Garlappi, L., Nogales, F. J., and Uppal, R. (2009). A generalized approach to portfolio optimization: Improving performance by constraining portfolio norms. *Management Science*, 55:798–812. 5, 5

Demsar, J. (2006). Statistical comparisons of classifiers over multiple data sets. *J. Mach. Learn. Res.*, 7:1–30. 3

Elton, E. J. and Gruber, M. J. (1973). Estimating the dependence structure of share prices– implications for portfolio selection. *The Journal of Finance*, 28(5):1203–1232. 1

Engle, R. (2002). Dynamic conditional correlation. *Journal of Business & Economic Statistics*, 20(3):339–350. 1, 2.3.2

Engle, R. F., Ledoit, O., and Wolf, M. (2019). Large dynamic covariance matrices. *Journal of Business & Economic Statistics*, 37(2):363–375. 1, 2.3.3

Engle, R. F. and Sheppard, K. (2001). Theoretical and empirical properties of dynamic conditional correlation multivariate garch. Working Paper 8554, National Bureau of Economic Research. 2.3.2

Fama, E. F. and French, K. R. (1993). Common risk factors in the returns on stocks and bonds. *Journal of financial economics*, 33(1):3–56. 1

Gu, S., Kelly, B., and Xiu, D. (2020). Empirical asset pricing via machine learning. *The Review of Financial Studies*, 33:2223–2273. 1

Hansen, B. E. (1994). Autoregressive conditional density estimation. *International Economic Review*, 35(3):705–730. 2

Harvey, A. (1997). Trends, cycles and autoregressions. *The Economic Journal*, 107(440):192–201. 2

Hochreiter, S. (1997). Long short-term memory. *Neural Computation MIT-Press*. 2.4.3, A.1

J.P.Morgan (1996). *Riskmetrics technical document*. Morgan Guaranty Trust Company of New York. 2.1.3

Kim, I., Lee, M., and Seok, J. (2023). Icegan: Inverse covariance estimating generative adversarial network. *Machine Learning: Science and Technology*, 4:025008. 1

Kourtis, A. (2014). On the distribution and estimation of trading costs. *Journal of Empirical Finance*, 28:104–117. 5

Kourtis, A., Dotsis, G., and Markellos, R. N. (2012). Parameter uncertainty in portfolio selection: Shrinking the inverse covariance matrix. *Journal of Banking & Finance*, 36(9):2522–2531. 5

Laloux, L., Cizeau, P., Potters, M., and Bouchaud, J.-P. (2000). Random matrix theory and financial correlations. *International Journal of Theoretical and Applied Finance*, 03:391–397. 1, 2.2.2

Lecun, Y., Bottou, L., Bengio, Y., and Haffner, P. (1998). Gradient-based learning applied to document recognition. *Proceedings of the IEEE*, 86(11):2278–2324. 2.4.2

Ledoit, O. and Wolf, M. (2003). Improved estimation of the covariance matrix of stock returns with an application to portfolio selection. *Journal of Empirical Finance*, 10(5):603–621. 1, 2.2.1

Ledoit, O. and Wolf, M. (2004). A well-conditioned estimator for large-dimensional covariance matrices. *Journal of Multivariate Analysis*, 88(2):365–411. 1, 2.2.3, 2.2.4

Ledoit, O. and Wolf, M. (2015). Spectrum estimation: A unified framework for covariance matrix estimation and pca in large dimensions. *Journal of Multivariate Analysis*, 139:360–384. 2.3.3

Ledoit, O. and Wolf, M. (2020). Analytical nonlinear shrinkage of large-dimensional covariance matrices. *The Annals of Statistics*, 48(5):3043 – 3065. 2.3.3

Ledoit, O. and Wolf, M. (2022). The power of (non-)linear shrinking: A review and guide to covariance matrix estimation. *Journal of Financial Econometrics*, 20:187–218. 1

Liu, G. and Guo, J. (2019). Bidirectional lstm with attention mechanism and convolutional layer for text classification. *Neurocomputing*, 337:325–338. 2.4.3

Markowitz, H. (1952). Portfolio selection. *The Journal of Finance*, 7:77–91. 1, 4.2

Nazaret, N. and Reddy, Y. V. R. (2023). Financial applications of machine learning: A literature review. *Expert Systems with Applications*, 219:119640. 1

Olorunnimbe, K. and Viktor, H. (2023). Deep learning in the stock market—a systematic survey of practice, backtesting, and applications. *Artificial Intelligence Review*, 56(3):2057–2109. 1

Reis, P., Serra, A. P., and Gama, J. (2024). The role of deep learning in financial asset management: A systematic review. *Authorea, Inc.* 1

Sandoval, L. and Franca, I. D. P. (2012). Correlation of financial markets in times of crisis. *Physica A: Statistical Mechanics and its Applications*, 391(1):187–208. 1

Symitsi, E., Symeonidis, L., Kourtis, A., and Markellos, R. (2018). Covariance forecasting in equity markets. *Journal of Banking & Finance*, 96:153–168. 1, 2.5, 5

Vaswani, A., Shazeer, N. M., Parmar, N., Uszkoreit, J., Jones, L., Gomez, A. N., Kaiser, L., and Polosukhin, I. (2017). Attention is all you need. In *Neural Information Processing Systems*. 1, 2.4.4

Zhang, C., Pu, X., Cucuringu, M., and Dong, X. (2024). Graph-based methods for forecasting realized covariances. *Journal of Financial Econometrics*, page nbae026. 1, 2.5

A Appendix

A.1 LSTM cell detailed explanation

An LSTM (Hochreiter, 1997) cell consists of three main gates: the forget gate (f_t), the input gate (i_t), and the output gate (o_t). They are respectively calculated as:

$$f_t = \sigma(\mathbf{W}_f.[\mathbf{h}_{(t-1)}, \mathbf{x}_t] + \mathbf{b}_f) \tag{A.1}$$

$$i_t = \sigma(\mathbf{W}_i.[\mathbf{h}_{(t-1)}, \mathbf{x}_t] + \mathbf{b}_i) \tag{A.2}$$

$$o_t = \sigma(\mathbf{W}_o.[\mathbf{h}_{(t-1)}, \mathbf{x}_t] + \mathbf{b}_o) \tag{A.3}$$

where $\mathbf{x}_t$ is the vector input at time t, $\mathbf{h}_{(t-1)}$ is the hidden vector state, $\mathbf{W}_f$, $\mathbf{W}_i$ and $\mathbf{W}_c$ are weight matrices, and $\mathbf{b}_f$, $\mathbf{b}_i$ and $\mathbf{b}_o$ are bias vectors. The sigmoid function σ ensures that the output values are between 0 and 1, representing how much each component should be forgotten.

The forget gate decides what information should be discarded from the cell state. Next, the input gate determines what new information should be added to the cell state. This process involves two steps: calculating the input gate Eq. (A.2) and creating new candidate values:

$$\widetilde{\mathbf{C}}_t = \tanh\left(\mathbf{W}_c \cdot [\mathbf{h}_{t-1}, \mathbf{x}_t] + \mathbf{b}_c\right) \tag{A.4}$$

where $\mathbf{W}_c$ is the weight matrix, and $\mathbf{b}_c$ is a bias vector. The input gate modulates the extent to which new information is added to the cell state. The cell state update combines the forget gate and input gate operations to update the cell state:

$$\mathbf{C}_t = f_t \odot \mathbf{C}_{(t-1)} + i_t \odot \widetilde{\mathbf{C}}_t \tag{A.5}$$

This equation ensures that the cell state retains essential information over long periods.

Finally, the output gate controls what information should be outputted from the cell. This involves two steps: calculating the output gate Eq. (A.3) and determining the hidden state:

$$\mathbf{h}_t = o_t \odot \tanh\left(\mathbf{C}_t\right) \tag{A.6}$$

A.2   Hyperparameter Grid Search

Table A1 – Hyperparameter Grid Search table.

Hyperparameter	Range
Optimiser	Adam, SGD
Batch size	32, 64, 128, 256
Learning rate	$10^{-3}, 10^{-4}, 10^{-5}$
Lookback window (L)	20, 40, 60, 80, 100, 120, 250
3D convolution kernel size (ks)	3, 5, 7
BiLSTM hidden dimensions (hd)	32, 64, 128, 256
BiLSTM stacked layers (u)	3, 4, 5, 6, 7
Number of heads (he)[a]	2, 4, 6, 8, 16, 32
Shrinkage factor (ϕ)	0.00, 0.20, 0.40, 0.60, 0.80, 1.00

A.3   Extended ETF List

Table A2 – List of ETFs used in the larger dataset.

Name	Ticker	Incept. Date	Asset Class
iShares Core International Aggregate Bond ETF	IAGG	10/11/2015	Fixed Income
iShares MSCI Saudi Arabia ETF	KSA	16/09/2015	Equity
iShares Interest Rate Hedged Long-Term Corporate Bond ETF	IGBH	22/07/2015	Fixed Income
iShares Currency Hedged MSCI ACWI ex U.S. ETF	HAWX	29/06/2015	Equity
iShares Currency Hedged MSCI EAFE Small-Cap ETF	HSCZ	29/06/2015	Equity
iShares MSCI Intl Value Factor ETF	IVLU	16/06/2015	Equity
iShares Convertible Bond ETF	ICVT	02/06/2015	Fixed Income
iShares U.S. Equity Factor ETF	LRGF	28/04/2015	Equity
iShares U.S. Small-Cap Equity Factor ETF	SMLF	28/04/2015	Equity
iShares International Equity Factor ETF	INTF	28/04/2015	Equity
iShares International Small-Cap Equity Factor ETF	ISCF	28/04/2015	Equity
iShares Global Equity Factor ETF	GLOF	28/04/2015	Equity
iShares Exponential Technologies ETF	XT	19/03/2015	Equity

Continued on next page

Name	Ticker	Incept. Date	Asset Class
iShares iBonds Dec 2025 Term Corporate ETF	IBDQ	11/03/2015	Fixed Income
iShares Short Maturity Municipal Bond Active ETF	MEAR	03/03/2015	Fixed Income
iShares U.S. Fixed Income Balanced Risk Systematic ETF	FIBR	24/02/2015	Fixed Income
iShares MSCI Intl Quality Factor ETF	IQLT	13/01/2015	Equity
iShares MSCI Intl Momentum Factor ETF	IMTM	13/01/2015	Equity
iShares MSCI ACWI Low Carbon Target ETF	CRBN	08/12/2014	Equity
iShares GSCI Commodity Dynamic Roll Strategy ETF	COMT	15/10/2014	Commodity
iShares Currency Hedged MSCI Emerging Markets ETF	HEEM	23/09/2014	Equity
iShares Currency Hedged MSCI Eurozone ETF	HEZU	09/07/2014	Equity
iShares Global REIT ETF	REET	08/07/2014	Real Estate
iShares Core Total USD Bond Market ETF	IUSB	10/06/2014	Fixed Income
iShares Core Dividend Growth ETF	DGRO	10/06/2014	Equity
iShares Core MSCI Europe ETF	IEUR	10/06/2014	Equity
iShares Core MSCI Pacific ETF	IPAC	10/06/2014	Equity
iShares Interest Rate Hedged Corporate Bond ETF	LQDH	27/05/2014	Fixed Income
iShares Interest Rate Hedged High Yield Bond ETF	HYGH	27/05/2014	Fixed Income
iShares MSCI UAE ETF	UAE	29/04/2014	Equity
iShares MSCI Qatar ETF	QAT	29/04/2014	Equity
iShares Yield Optimized Bond ETF	BYLD	22/04/2014	Fixed Income
iShares Treasury Floating Rate Bond ETF	TFLO	03/02/2014	Fixed Income
iShares Currency Hedged MSCI EAFE ETF	HEFA	31/01/2014	Equity
iShares Currency Hedged MSCI Japan ETF	HEWJ	31/01/2014	Equity
iShares Ultra Short-Term Bond Active ETF	ICSH	11/12/2013	Fixed Income
iShares 0-5 Year High Yield Corporate Bond ETF	SHYG	15/10/2013	Fixed Income
iShares 0-5 Year Investment Grade Corporate Bond ETF	SLQD	15/10/2013	Fixed Income
iShares Short Duration Bond Active ETF	NEAR	25/09/2013	Fixed Income
iShares MSCI USA Quality Factor ETF	QUAL	16/07/2013	Equity
iShares MSCI USA Momentum Factor ETF	MTUM	16/04/2013	Equity
iShares MSCI USA Value Factor ETF	VLUE	16/04/2013	Equity
iShares MSCI USA Size Factor ETF	SIZE	16/04/2013	Equity

Name	Ticker	Incept. Date	Asset Class
iShares Core MSCI EAFE ETF	IEFA	18/10/2012	Equity
iShares Core MSCI Emerging Markets ETF	IEMG	18/10/2012	Equity
iShares Core MSCI Total International Stock ETF	IXUS	18/10/2012	Equity
iShares Core 1-5 Year USD Bond ETF	ISTB	18/10/2012	Fixed Income
iShares J.P. Morgan EM Corporate Bond ETF	CEMB	17/04/2012	Fixed Income
iShares J.P. Morgan EM High Yield Bond ETF	EMHY	03/04/2012	Fixed Income
iShares US & Intl High Yield Corp Bond ETF	GHYG	03/04/2012	Fixed Income
iShares Morningstar Multi-Asset Income ETF	IYLD	03/04/2012	Multi Asset
iShares International High Yield Bond ETF	HYXU	03/04/2012	Fixed Income
iShares Emerging Markets Dividend ETF	DVYE	23/02/2012	Equity
iShares Asia/Pacific Dividend ETF	DVYA	23/02/2012	Equity
iShares U.S. Treasury Bond ETF	GOVT	14/02/2012	Fixed Income
iShares Aaa - A Rated Corporate Bond ETF	QLTA	14/02/2012	Fixed Income
iShares CMBS ETF	CMBS	14/02/2012	Others
iShares GNMA Bond ETF	GNMA	14/02/2012	Fixed Income
iShares MSCI India Small-Cap ETF	SMIN	08/02/2012	Equity
iShares MSCI Emerging Markets Asia ETF	EEMA	08/02/2012	Equity
iShares MSCI India ETF	INDA	02/02/2012	Equity
iShares MSCI Global Gold Miners ETF	RING	31/01/2012	Equity
iShares MSCI Global Metals & Mining Producers ETF	PICK	31/01/2012	Equity
iShares MSCI Global Silver and Metals Miners ETF	SLVP	31/01/2012	Equity
iShares MSCI Agriculture Producers ETF	VEGI	31/01/2012	Equity
iShares MSCI Global Energy Producers ETF	FILL	31/01/2012	Equity
iShares MSCI Denmark ETF	EDEN	25/01/2012	Equity
iShares MSCI United Kingdom Small-Cap ETF	EWUS	25/01/2012	Equity
iShares MSCI Finland ETF	EFNL	25/01/2012	Equity
iShares MSCI Norway ETF	ENOR	23/01/2012	Equity
iShares MSCI World ETF	URTH	10/01/2012	Equity
iShares MSCI USA Min Vol Factor ETF	USMV	18/10/2011	Equity
iShares MSCI EAFE Min Vol Factor ETF	EFAV	18/10/2011	Equity

Continued on next page

Name	Ticker	Incept. Date	Asset Class
iShares MSCI Global Min Vol Factor ETF	ACWV	18/10/2011	Equity
iShares MSCI Emerging Markets Min Vol Factor ETF	EEMV	18/10/2011	Equity
iShares J.P. Morgan EM Local Currency Bond ETF	LEMB	18/10/2011	Fixed Income
iShares MSCI Emerging Markets Small-Cap ETF	EEMS	16/08/2011	Equity
iShares Floating Rate Bond ETF	FLOT	14/06/2011	Fixed Income
iShares Core High Dividend ETF	HDV	29/03/2011	Equity
iShares MSCI China ETF	MCHI	29/03/2011	Equity
iShares 0-5 Year TIPS Bond ETF	STIP	01/12/2010	Fixed Income
iShares MSCI Brazil Small-Cap ETF	EWZS	28/09/2010	Equity
iShares MSCI Philippines ETF	EPHE	28/09/2010	Equity
iShares MSCI China Small-Cap ETF	ECNS	28/09/2010	Equity
iShares MSCI New Zealand ETF	ENZL	01/09/2010	Equity
iShares MSCI Poland ETF	EPOL	25/05/2010	Equity
iShares MSCI USA Equal Weighted ETF	EUSA	05/05/2010	Equity
iShares MSCI Indonesia ETF	EIDO	05/05/2010	Equity
iShares MSCI Ireland ETF	EIRL	05/05/2010	Equity
iShares MSCI Europe Financials ETF	EUFN	20/01/2010	Equity
iShares 10+ Year Investment Grade Corporate Bond ETF	IGLB	08/12/2009	Fixed Income
iShares Core 10+ Year USD Bond ETF	ILTB	08/12/2009	Fixed Income
iShares India 50 ETF	INDY	18/11/2009	Equity
iShares Russell Top 200 Growth ETF	IWY	22/09/2009	Equity
iShares Russell Top 200 Value ETF	IWX	22/09/2009	Equity
iShares Russell Top 200 ETF	IWL	22/09/2009	Equity
iShares MSCI Peru and Global Exposure ETF	EPU	19/06/2009	Equity
iShares Emerging Markets Infrastructure ETF	EMIF	16/06/2009	Equity
iShares International Treasury Bond ETF	IGOV	21/01/2009	Fixed Income
iShares 1-3 Year International Treasury Bond ETF	ISHG	21/01/2009	Fixed Income
iShares Short-Term National Muni Bond ETF	SUB	05/11/2008	Fixed Income
iShares Agency Bond ETF	AGZ	05/11/2008	Fixed Income
iShares Core Growth Allocation ETF	AOR	04/11/2008	Multi Asset

Continued on next page

Name	Ticker	Incept. Date	Asset Class
iShares Core Aggressive Allocation ETF	AOA	04/11/2008	Multi Asset
iShares Core Moderate Allocation ETF	AOM	04/11/2008	Multi Asset
iShares Core Conservative Allocation ETF	AOK	04/11/2008	Multi Asset
iShares MSCI All Country Asia ex Japan ETF	AAXJ	13/08/2008	Equity
iShares Global Clean Energy ETF	ICLN	24/06/2008	Equity
iShares Global Timber & Forestry ETF	WOOD	24/06/2008	Equity
iShares MSCI ACWI ETF	ACWI	26/03/2008	Equity
iShares MSCI ACWI ex U.S. ETF	ACWX	26/03/2008	Equity
iShares MSCI Israel ETF	EIS	26/03/2008	Equity
iShares MSCI Thailand ETF	THD	26/03/2008	Equity
iShares MSCI Turkey ETF	TUR	26/03/2008	Equity
iShares MSCI Japan Small-Cap ETF	SCJ	20/12/2007	Equity
iShares J.P. Morgan USD Emerging Markets Bond ETF	EMB	17/12/2007	Fixed Income
iShares MSCI EAFE Small-Cap ETF	SCZ	10/12/2007	Equity
iShares Global Infrastructure ETF	IGF	10/12/2007	Equity
iShares MSCI Kokusai ETF	TOK	10/12/2007	Equity
iShares Asia 50 ETF	AIA	13/11/2007	Equity
iShares MSCI Chile ETF	ECH	12/11/2007	Equity
iShares International Developed Real Estate ETF	IFGL	12/11/2007	Real Estate
iShares MSCI Europe Small-Cap ETF	IEUS	12/11/2007	Equity
iShares MSCI BIC ETF	BKF	12/11/2007	Equity
iShares California Muni Bond ETF	CMF	04/10/2007	Fixed Income
iShares New York Muni Bond ETF	NYF	04/10/2007	Fixed Income
iShares National Muni Bond ETF	MUB	07/09/2007	Fixed Income
iShares International Select Dividend ETF	IDV	11/06/2007	Equity
iShares Core U.S. REIT ETF	USRT	01/05/2007	Real Estate
iShares Residential and Multisector Real Estate ETF	REZ	01/05/2007	Real Estate
iShares Mortgage Real Estate ETF	REM	01/05/2007	Real Estate
iShares iBoxx High Yield Corporate Bond ETF	HYG	04/04/2007	Fixed Income
iShares Preferred and Income Securities ETF	PFF	26/03/2007	Equity

Name	Ticker	Incept. Date	Asset Class
iShares MBS ETF	MBB	13/03/2007	Fixed Income
iShares 1-5 Year Investment Grade Corporate Bond ETF	IGSB	05/01/2007	Fixed Income
iShares Short Treasury Bond ETF	SHV	05/01/2007	Fixed Income
iShares 3-7 Year Treasury Bond ETF	IEI	05/01/2007	Fixed Income
iShares 5-10 Year Investment Grade Corporate Bond ETF	IGIB	05/01/2007	Fixed Income
iShares Broad USD Investment Grade Corporate Bond ETF	USIG	05/01/2007	Fixed Income
iShares 10-20 Year Treasury Bond ETF	TLH	05/01/2007	Fixed Income
iShares Intermediate Government/Credit Bond ETF	GVI	05/01/2007	Fixed Income
iShares Government/Credit Bond ETF	GBF	05/01/2007	Fixed Income
iShares MSCI KLD 400 Social ETF	DSI	14/11/2006	Equity
iShares Global Industrials ETF	EXI	12/09/2006	Equity
iShares Global Consumer Staples ETF	KXI	12/09/2006	Equity
iShares Global Consumer Discretionary ETF	RXI	12/09/2006	Equity
iShares Global Materials ETF	MXI	12/09/2006	Equity
iShares Global Utilities ETF	JXI	12/09/2006	Equity
iShares S&P GSCI Commodity-Indexed Trust	GSG	10/07/2006	Commodity
iShares U.S. Aerospace & Defense ETF	ITA	01/05/2006	Equity
iShares U.S. Medical Devices ETF	IHI	01/05/2006	Equity
iShares U.S. Home Construction ETF	ITB	01/05/2006	Equity
iShares U.S. Broker-Dealers & Securities Exchanges ETF	IAI	01/05/2006	Equity
iShares U.S. Regional Banks ETF	IAT	01/05/2006	Equity
iShares U.S. Insurance ETF	IAK	01/05/2006	Equity
iShares U.S. Healthcare Providers ETF	IHF	01/05/2006	Equity
iShares U.S. Pharmaceuticals ETF	IHE	01/05/2006	Equity
iShares U.S. Oil & Gas Exploration & Production ETF	IEO	01/05/2006	Equity
iShares U.S. Oil Equipment & Services ETF	IEZ	01/05/2006	Equity
iShares Silver Trust	SLV	21/04/2006	Commodity
iShares Micro-Cap ETF	IWC	12/08/2005	Equity
iShares MSCI EAFE Value ETF	EFV	01/08/2005	Equity
iShares MSCI EAFE Growth ETF	EFG	01/08/2005	Equity

Name	Ticker	Incept. Date	Asset Class
iShares MSCI USA ESG Select ETF	SUSA	24/01/2005	Equity
iShares Gold Trust	IAU	21/01/2005	Commodity
iShares China Large-Cap ETF	FXI	05/10/2004	Equity
iShares Morningstar Mid-Cap Growth ETF	IMCG	28/06/2004	Equity
iShares Morningstar Growth ETF	ILCG	28/06/2004	Equity
iShares Morningstar U.S. Equity ETF	ILCB	28/06/2004	Equity
iShares Morningstar Mid-Cap ETF	IMCB	28/06/2004	Equity
iShares Morningstar Value ETF	ILCV	28/06/2004	Equity
iShares Morningstar Mid-Cap Value ETF	IMCV	28/06/2004	Equity
iShares Morningstar Small-Cap Growth ETF	ISCG	28/06/2004	Equity
iShares Morningstar Small-Cap Value ETF	ISCV	28/06/2004	Equity
iShares Morningstar Small-Cap ETF	ISCB	28/06/2004	Equity
iShares Core S&P Total U.S. Stock Market ETF	ITOT	20/01/2004	Equity
iShares TIPS Bond ETF	TIP	04/12/2003	Fixed Income
iShares Select Dividend ETF	DVY	03/11/2003	Equity
iShares U.S. Transportation ETF	IYT	06/10/2003	Equity
iShares Core U.S. Aggregate Bond ETF	AGG	22/09/2003	Fixed Income
iShares MSCI Emerging Markets ETF	EEM	07/04/2003	Equity
iShares MSCI South Africa ETF	EZA	03/02/2003	Equity
iShares 20+ Year Treasury Bond ETF	TLT	22/07/2002	Fixed Income
iShares 7-10 Year Treasury Bond ETF	IEF	22/07/2002	Fixed Income
iShares iBoxx Investment Grade Corporate Bond ETF	LQD	22/07/2002	Fixed Income
iShares 1-3 Year Treasury Bond ETF	SHY	22/07/2002	Fixed Income
iShares Global Healthcare ETF	IXJ	13/11/2001	Equity
iShares Global Tech ETF	IXN	12/11/2001	Equity
iShares Global Energy ETF	IXC	12/11/2001	Equity
iShares Global Financials ETF	IXG	12/11/2001	Equity
iShares Global Comm Services ETF	IXP	12/11/2001	Equity
iShares MSCI Pacific ex Japan ETF	EPP	25/10/2001	Equity
iShares Latin America 40 ETF	ILF	25/10/2001	Equity

Name	Ticker	Incept. Date	Asset Class
iShares JPX-Nikkei 400 ETF	JPXN	23/10/2001	Equity
iShares North American Natural Resources ETF	IGE	22/10/2001	Equity
iShares MSCI EAFE ETF	EFA	14/08/2001	Equity
iShares Russell Mid-Cap ETF	IWR	17/07/2001	Equity
iShares Russell Mid-Cap Growth ETF	IWP	17/07/2001	Equity
iShares Russell Mid-Cap Value ETF	IWS	17/07/2001	Equity
iShares Semiconductor ETF	SOXX	10/07/2001	Equity
iShares Expanded Tech-Software Sector ETF	IGV	10/07/2001	Equity
iShares U.S. Digital Infrastructure and Real Estate ETF	IDGT	10/07/2001	Equity
iShares Expanded Tech Sector ETF	IGM	13/03/2001	Equity
iShares Biotechnology ETF	IBB	05/02/2001	Equity
iShares Cohen & Steers REIT ETF	ICF	29/01/2001	Real Estate
iShares Global 100 ETF	IOO	05/12/2000	Equity
iShares S&P 100 ETF	OEF	23/10/2000	Equity
iShares MSCI Eurozone ETF	EZU	25/07/2000	Equity
iShares Europe ETF	IEV	25/07/2000	Equity
iShares Core S&P U.S. Growth ETF	IUSG	24/07/2000	Equity
iShares Core S&P U.S. Value ETF	IUSV	24/07/2000	Equity
iShares Russell 2000 Growth ETF	IWO	24/07/2000	Equity
iShares Russell 2000 Value ETF	IWN	24/07/2000	Equity
iShares S&P Mid-Cap 400 Growth ETF	IJK	24/07/2000	Equity
iShares S&P Mid-Cap 400 Value ETF	IJJ	24/07/2000	Equity
iShares S&P Small-Cap 600 Value ETF	IJS	24/07/2000	Equity
iShares S&P Small-Cap 600 Growth ETF	IJT	24/07/2000	Equity
iShares MSCI Brazil ETF	EWZ	10/07/2000	Equity
iShares MSCI Taiwan ETF	EWT	20/06/2000	Equity
iShares U.S. Real Estate ETF	IYR	12/06/2000	Real Estate
iShares U.S. Healthcare ETF	IYH	12/06/2000	Equity
iShares Dow Jones U.S. ETF	IYY	12/06/2000	Equity
iShares U.S. Consumer Discretionary ETF	IYC	12/06/2000	Equity

Name	Ticker	Incept. Date	Asset Class
iShares U.S. Financial Services ETF	IYG	12/06/2000	Equity
iShares U.S. Industrials ETF	IYJ	12/06/2000	Equity
iShares U.S. Energy ETF	IYE	12/06/2000	Equity
iShares U.S. Consumer Staples ETF	IYK	12/06/2000	Equity
iShares U.S. Utilities ETF	IDU	12/06/2000	Equity
iShares U.S. Basic Materials ETF	IYM	12/06/2000	Equity
iShares Russell 1000 Growth ETF	IWF	22/05/2000	Equity
iShares Core S&P Mid-Cap ETF	IJH	22/05/2000	Equity
iShares Core S&P Small-Cap ETF	IJR	22/05/2000	Equity
iShares Russell 2000 ETF	IWM	22/05/2000	Equity
iShares Russell 1000 Value ETF	IWD	22/05/2000	Equity
iShares S&P 500 Growth ETF	IVW	22/05/2000	Equity
iShares S&P 500 Value ETF	IVE	22/05/2000	Equity
iShares Russell 3000 ETF	IWV	22/05/2000	Equity
iShares U.S. Financials ETF	IYF	22/05/2000	Equity
iShares U.S. Telecommunications ETF	IYZ	22/05/2000	Equity
iShares Core S&P 500 ETF	IVV	15/05/2000	Equity
iShares Russell 1000 ETF	IWB	15/05/2000	Equity
iShares U.S. Technology ETF	IYW	15/05/2000	Equity
iShares MSCI South Korea ETF	EWY	09/05/2000	Equity
iShares MSCI Japan ETF	EWJ	12/03/1996	Equity
iShares MSCI United Kingdom ETF	EWU	12/03/1996	Equity
iShares MSCI Canada ETF	EWC	12/03/1996	Equity
iShares MSCI Australia ETF	EWA	12/03/1996	Equity
iShares MSCI Mexico ETF	EWW	12/03/1996	Equity
iShares MSCI Switzerland ETF	EWL	12/03/1996	Equity
iShares MSCI Germany ETF	EWG	12/03/1996	Equity
iShares MSCI Spain ETF	EWP	12/03/1996	Equity
iShares MSCI Singapore ETF	EWS	12/03/1996	Equity
iShares MSCI Hong Kong ETF	EWH	12/03/1996	Equity

Name	Ticker	Incept. Date	Asset Class
iShares MSCI France ETF	EWQ	12/03/1996	Equity
iShares MSCI Italy ETF	EWI	12/03/1996	Equity
iShares MSCI Sweden ETF	EWD	12/03/1996	Equity
iShares MSCI Malaysia ETF	EWM	12/03/1996	Equity
iShares MSCI Netherlands ETF	EWN	12/03/1996	Equity
iShares MSCI Austria ETF	EWO	12/03/1996	Equity
iShares MSCI Belgium ETF	EWK	12/03/1996	Equity

A.4 Extended Tables

Table A3 – Average Euclidean ($\mathcal{L}^E$) and Frobenius ($\mathcal{L}^F$) distances ($\times 10^5$) using *excess* returns with different horizons (F) for different testing periods: Overall (1 January 2021 to 31 December 2023), Bull-1 (1 January 2021 to 2 January 2022), Bear (3 January 2022 to 12 June 2022), and Bull-2 (13 June 2022 to 31 December 2023).

		Overall		Bull-1		Bear		Bull-2	
		$\mathcal{L}^E$	$\mathcal{L}^F$	$\mathcal{L}^E$	$\mathcal{L}^F$	$\mathcal{L}^E$	$\mathcal{L}^F$	$\mathcal{L}^E$	$\mathcal{L}^F$
	NA	70.309	107.739	54.194	82.600	107.447	165.092	69.960	107.363
	NA^F	62.260	95.586	46.956	71.921	106.652	163.471	59.271	91.185
	$EWMA$	58.851	90.253	**42.125**	**64.612**	<u>94.704</u>	**145.253**	59.272	90.889
	PCA	71.266	109.164	54.984	83.752	110.811	170.301	70.323	107.864
$F = 10$	RMT	71.064	108.951	54.819	83.588	110.623	170.011	70.094	107.641
	LW	63.548	97.681	47.376	72.757	104.804	160.926	62.036	95.449
	LW^F	75.861	115.370	69.194	104.027	105.832	162.356	71.461	109.054
	CCC	<u>58.111</u>	<u>89.824</u>	<u>42.451</u>	<u>65.818</u>	95.819	147.003	<u>57.301</u>	<u>88.763</u>
	DCC	62.210	95.018	48.557	73.797	96.913	147.989	60.972	93.374
	DCC^{NL}	65.361	99.154	51.461	77.640	100.48	152.649	64.160	97.548
	CAB	**56.954**	**87.317**	44.134	67.401	**94.689**	<u>145.287</u>	**54.291**	**83.369**

Continued on next page

		$\mathcal{L}^E$	$\mathcal{L}^F$	$\mathcal{L}^E$	$\mathcal{L}^F$	$\mathcal{L}^E$	$\mathcal{L}^F$	$\mathcal{L}^E$	$\mathcal{L}^F$
$F = 40$	NA	45.872	70.272	24.755	38.850	72.135	108.838	51.939	79.449
	NA^F	47.436	72.906	31.056	47.811	90.540	139.813	45.522	69.719
	$EWMA$	44.734	68.528	26.175	40.546	74.009	112.405	48.262	73.923
	PCA	46.390	71.007	24.934	39.238	72.294	109.567	52.781	80.410
	RMT	46.177	70.771	24.796	39.028	72.411	109.269	52.424	80.176
	LW	43.441	66.728	23.834	37.275	76.162	114.702	46.645	71.886
	LW^F	63.848	96.730	62.374	93.125	78.628	122.264	60.501	91.635
	CCC	43.434	67.183	27.608	43.493	75.190	114.891	44.465	68.675
	DCC	42.622	66.124	27.194	42.996	73.983	113.348	43.509	67.391
	DCC^{NL}	43.764	67.604	28.135	44.201	75.173	114.919	44.767	69.024
	CAB	**22.851**	**35.411**	**13.091**	**20.268**	**42.372**	**65.754**	**23.505**	**36.408**
$F = 60$	NA	44.053	68.114	26.115	42.593	72.110	109.681	47.531	72.584
	NA^F	45.519	69.961	30.907	47.659	83.084	128.667	44.068	67.348
	$EWMA$	44.704	68.490	26.626	41.728	74.557	112.995	47.751	72.910
	PCA	44.550	68.801	26.466	43.142	72.705	111.010	48.096	73.173
	RMT	44.334	68.575	26.291	42.936	72.803	110.768	47.761	72.940
	LW	42.035	65.084	24.836	40.385	75.018	113.948	43.600	66.895
	LW^F	62.001	93.989	62.649	93.590	69.286	108.383	59.458	90.055
	CCC	42.647	66.037	29.089	45.917	68.525	105.242	43.916	67.686
	DCC	40.986	63.934	26.426	42.585	69.459	106.517	42.150	65.398
	DCC^{NL}	42.268	65.595	27.106	43.443	71.582	109.283	43.579	67.259
	CAB	**22.305**	**34.990**	**12.842**	**20.226**	**39.166**	**62.879**	**23.540**	**36.458**
$F = 90$	NA	43.972	68.530	30.179	49.646	76.424	117.032	43.479	66.670
	NA^F	43.572	67.004	30.527	47.207	83.143	128.419	40.520	61.975
	$EWMA$	44.720	68.781	28.925	45.742	73.402	111.890	46.624	71.190
	PCA	44.464	69.171	30.520	50.091	76.867	118.267	44.085	67.265
	RMT	44.239	68.951	30.343	49.925	77.105	118.060	43.693	67.005

		$\mathcal{L}^E$	$\mathcal{L}^F$	$\mathcal{L}^E$	$\mathcal{L}^F$	$\mathcal{L}^E$	$\mathcal{L}^F$	$\mathcal{L}^E$	$\mathcal{L}^F$
$F = 90$	LW	42.446	66.204	28.694	47.283	79.704	121.665	40.527	62.340
	LW^F	60.006	91.073	61.704	92.289	64.055	100.713	57.724	87.477
	CCC	43.390	67.342	32.735	51.757	68.495	105.076	42.999	66.475
	DCC	40.234	63.342	29.961	48.303	65.688	101.473	39.492	62.005
	DCC^{NL}	42.615	66.462	29.762	48.148	71.380	108.855	42.584	66.011
	CAB	**13.977**	**21.752**	**10.080**	**16.184**	**20.742**	**32.133**	**14.538**	**22.346**
$F = 120$	NA	48.590	75.398	36.397	59.019	84.342	128.425	46.097	70.593
	NA^F	41.909	64.465	31.713	49.127	84.615	129.958	36.093	55.352
	EWMA	45.330	69.861	33.556	53.195	71.953	109.497	45.222	69.142
	PCA	49.115	76.015	36.715	59.374	84.740	129.651	46.794	71.202
	RMT	48.867	75.827	36.519	59.220	85.041	129.486	46.352	70.985
	LW	47.098	73.175	34.956	56.786	87.296	132.635	43.277	66.502
	LW^F	58.216	88.420	60.114	90.286	64.569	100.736	55.133	83.621
	CCC	44.163	68.631	36.440	57.692	71.518	108.718	41.212	64.060
	DCC	40.946	64.563	33.741	54.358	68.094	104.261	37.719	59.629
	DCC^{NL}	44.082	68.671	34.120	54.937	74.174	112.239	41.789	64.902
	CAB	**12.635**	**19.816**	**10.718**	**17.319**	**18.659**	**29.190**	**12.125**	**18.707**
$F = 180$	NA	57.475	88.882	50.083	79.438	92.682	140.191	52.022	80.073
	NA^F	38.460	59.180	32.171	49.910	82.117	124.805	29.829	46.088
	EWMA	50.035	77.019	43.437	68.307	76.903	116.122	46.487	71.288
	PCA	58.026	89.446	50.494	79.976	92.884	141.079	52.765	80.559
	RMT	57.744	89.294	50.351	79.843	93.189	140.964	52.223	80.384
	LW	56.137	86.937	49.005	77.757	94.604	142.932	49.567	76.591
	LW^F	54.308	82.570	54.261	81.972	45.646	95.111	52.187	79.306
	CCC	44.949	70.232	40.531	64.242	72.901	110.150	39.678	62.498
	DCC	46.528	72.381	41.217	65.244	75.945	114.305	41.410	64.807
	DCC^{NL}	46.532	72.386	41.220	65.248	75.950	114.312	41.414	64.812
	CAB	**12.356**	**19.146**	**11.116**	**17.602**	**18.159**	**27.468**	**11.472**	**17.726**

Continued on next page

	$\mathcal{L}^E$	$\mathcal{L}^F$	$\mathcal{L}^E$	$\mathcal{L}^F$	$\mathcal{L}^E$	$\mathcal{L}^F$	$\mathcal{L}^E$	$\mathcal{L}^F$
NA	76.850	117.44	107.237	163.541	79.505	120.16	56.341	86.706
NA^F	<u>34.002</u>	<u>52.367</u>	<u>33.076</u>	<u>51.123</u>	64.126	97.309	25.830	<u>40.087</u>
PCA	77.628	118.284	108.476	165.211	79.544	120.791	57.035	87.075
RMT	77.315	118.139	108.26	165.074	79.841	120.668	56.481	86.919
$EWMA$	53.737	82.720	53.030	82.554	72.648	109.762	48.689	74.953
LW	74.903	114.697	103.984	158.986	80.825	122.029	54.291	83.797
LW^F	49.653	75.499	47.293	71.542	<u>45.646</u>	<u>70.522</u>	52.353	79.519
CCC	43.487	68.479	42.628	67.459	58.966	89.895	39.537	62.904
DCC	40.299	64.494	38.892	62.869	53.375	82.622	37.405	60.269
DCC^{NL}	40.223	66.604	49.514	77.717	81.610	120.697	<u>22.135</u>	43.633
CAB	**16.116**	**24.758**	**22.511**	**34.543**	**16.201**	**24.572**	**11.938**	**18.457**

(F = 250)

Table A4 – Average Euclidean ($\mathcal{L}^E$) and Frobenius ($\mathcal{L}^F$) distances ($\times 10^5$) using *raw* returns with different horizons (F) for different testing periods: Overall (1 January 2021 to 31 December 2023), Bull-1 (1 January 2021 to 2 January 2022), Bear (3 January 2022 to 12 June 2022), and Bull-2 (13 June 2022 to 31 December 2023).

	Overall		Bull-1		Bear		Bull-2	
	$\mathcal{L}^E$	$\mathcal{L}^F$	$\mathcal{L}^E$	$\mathcal{L}^F$	$\mathcal{L}^E$	$\mathcal{L}^F$	$\mathcal{L}^E$	$\mathcal{L}^F$
NA	70.309	107.739	54.193	82.599	107.449	165.094	69.959	107.362
NA^F	62.057	95.297	46.340	71.028	107.068	164.102	59.155	91.020
$EWMA$	58.908	90.338	**42.125**	**64.612**	<u>94.704</u>	<u>145.253</u>	59.384	91.053
PCA	71.265	109.164	54.983	83.750	110.813	170.304	70.322	107.863
RMT	71.064	108.951	54.818	83.587	110.625	170.014	70.093	107.640
LW	63.547	97.680	47.376	72.755	104.804	160.927	62.035	95.448
LW^F	75.854	115.361	69.181	104.007	105.831	162.355	71.457	109.048
CCC	**58.092**	<u>89.783</u>	<u>42.384</u>	<u>65.733</u>	95.843	147.035	57.300	88.730
DCC	62.186	94.973	48.470	73.686	96.894	147.968	60.986	93.364
DCC^{NL}	65.338	99.111	51.367	77.516	100.447	152.608	64.186	97.557
CAB	<u>58.272</u>	**89.475**	43.967	67.109	**94.554**	**145.032**	**56.996**	**87.822**

(F = 10)

Continued on next page

49

	$\mathcal{L}^E$	$\mathcal{L}^F$	$\mathcal{L}^E$	$\mathcal{L}^F$	$\mathcal{L}^E$	$\mathcal{L}^F$	$\mathcal{L}^E$	$\mathcal{L}^F$
$F=40$								
NA	45.876	70.278	24.754	38.850	<u>72.131</u>	<u>108.833</u>	51.948	79.462
NA^F	47.200	72.577	30.161	46.526	91.426	141.121	45.386	69.534
$EWMA$	44.796	68.618	26.174	40.545	74.005	112.399	48.383	74.100
PCA	46.394	71.012	24.934	39.237	72.291	109.562	52.789	80.423
RMT	46.181	70.777	24.796	39.027	72.408	109.265	52.432	80.188
LW	43.444	66.733	<u>23.834</u>	<u>37.275</u>	76.161	114.700	46.652	71.896
LW^F	63.845	96.725	62.359	93.102	78.638	122.279	60.502	91.636
CCC	43.321	67.023	27.469	43.276	75.123	114.858	44.354	68.515
DCC	<u>42.585</u>	<u>66.060</u>	27.081	42.811	74.082	113.527	<u>43.481</u>	<u>67.335</u>
DCC^{NL}	43.739	67.556	28.016	44.008	75.278	115.106	44.766	69.003
CAB	**26.619**	**41.417**	**13.427**	**20.765**	**45.197**	**69.510**	**29.777**	**46.649**
$F=60$								
NA	44.060	68.125	26.115	42.593	72.109	109.679	47.545	72.605
NA^F	45.268	69.612	30.016	46.385	84.049	130.081	43.879	67.086
$EWMA$	44.759	68.570	26.625	41.727	74.548	112.981	47.861	73.069
PCA	44.557	68.811	26.466	43.142	72.705	111.009	48.109	73.194
RMT	44.341	68.586	26.291	42.935	72.803	110.767	47.775	72.961
LW	42.043	65.095	<u>24.836</u>	<u>40.385</u>	75.020	113.951	43.615	66.916
LW^F	62.000	93.988	62.634	93.568	69.301	108.405	59.462	90.061
CCC	42.543	65.895	28.943	45.693	68.234	104.807	43.895	67.683
DCC	<u>39.404</u>	<u>61.909</u>	26.764	42.978	<u>64.589</u>	<u>100.135</u>	<u>40.279</u>	<u>63.072</u>
DCC^{NL}	42.240	65.544	27.015	43.295	71.326	108.855	43.658	67.380
CAB	**24.079**	**37.328**	**13.698**	**21.649**	**43.977**	**68.513**	**25.026**	**38.428**
$F=90$								
NA	43.982	68.545	30.179	49.646	76.435	117.049	43.496	66.694
NA^F	43.314	66.645	29.713	46.043	84.231	130.003	40.232	<u>61.574</u>
$EWMA$	44.761	68.841	28.925	<u>45.742</u>	73.405	111.893	46.704	71.306
PCA	44.474	69.186	30.520	50.092	76.878	118.284	44.100	67.288
RMT	44.249	68.966	30.343	49.925	77.116	118.077	43.709	67.029

		$\mathcal{L}^E$	$\mathcal{L}^F$	$\mathcal{L}^E$	$\mathcal{L}^F$	$\mathcal{L}^E$	$\mathcal{L}^F$	$\mathcal{L}^E$	$\mathcal{L}^F$
$F = 90$	LW	42.457	66.219	<u>28.694</u>	47.283	79.715	121.682	40.544	62.365
	LW^F	60.007	91.075	61.690	92.268	<u>64.073</u>	<u>100.740</u>	57.731	87.486
	CCC	43.276	67.199	32.551	51.513	68.021	104.421	43.036	66.546
	DCC	<u>40.134</u>	<u>63.219</u>	29.870	48.186	65.191	100.793	<u>39.503</u>	62.039
	DCC^{NL}	42.532	66.357	29.680	48.045	70.880	108.147	42.622	66.080
	CAB	**14.661**	**23.076**	**10.115**	**16.203**	**22.040**	**34.086**	**15.465**	**24.333**
$F = 120$	NA	48.604	75.417	36.397	59.018	84.366	128.460	46.116	70.620
	NA^F	<u>41.664</u>	<u>64.124</u>	<u>31.048</u>	<u>48.181</u>	85.754	131.620	<u>35.717</u>	<u>54.821</u>
	$EWMA$	45.361	69.908	33.555	53.194	71.959	109.504	45.282	69.232
	PCA	49.129	76.034	36.715	59.373	84.764	129.686	46.813	71.230
	RMT	48.881	75.846	36.519	59.219	85.065	129.521	46.371	71.013
	LW	47.111	73.194	34.955	56.785	87.320	132.670	43.296	66.530
	LW^F	58.219	88.425	60.101	90.267	<u>64.599</u>	<u>100.781</u>	55.138	83.629
	CCC	44.126	68.610	36.335	57.587	71.120	108.182	41.325	64.245
	DCC	43.988	68.569	34.032	54.862	73.636	111.512	41.819	64.965
	DCC^{NL}	44.025	68.619	34.051	54.887	73.690	111.582	41.864	65.025
	CAB	**12.118**	**18.831**	**9.496**	**15.248**	**17.864**	**27.435**	**12.147**	**18.653**
$F = 180$	NA	57.494	88.910	50.085	79.441	92.730	140.261	52.044	80.105
	NA^F	<u>38.294</u>	<u>58.953</u>	<u>31.839</u>	<u>49.444</u>	83.328	126.577	<u>29.370</u>	<u>45.434</u>
	$EWMA$	50.062	77.060	43.438	68.309	76.943	116.140	46.536	71.363
	PCA	58.045	89.474	50.496	79.979	92.932	141.148	52.787	80.592
	RMT	57.763	89.322	50.352	79.846	93.237	141.034	52.245	80.416
	LW	56.156	86.964	49.007	77.759	94.651	143.001	49.589	76.623
	LW^F	54.314	82.579	54.255	81.962	<u>61.748</u>	<u>95.188</u>	52.188	79.307
	CCC	44.844	70.073	40.368	64.069	72.299	109.109	39.755	62.603
	DCC	46.364	72.137	41.041	65.057	75.312	113.195	41.391	64.777
	DCC^{NL}	46.406	72.191	41.077	65.104	75.366	113.267	41.432	64.830
	CAB	**12.828**	**19.854**	**11.180**	**17.728**	**20.372**	**30.851**	**11.702**	**18.031**

Continued on next page

	$\mathcal{L}^E$	$\mathcal{L}^F$	$\mathcal{L}^E$	$\mathcal{L}^F$	$\mathcal{L}^E$	$\mathcal{L}^F$	$\mathcal{L}^E$	$\mathcal{L}^F$
NA	76.900	117.511	107.237	163.540	79.568	120.252	56.420	86.818
NA^F	<u>34.000</u>	<u>52.376</u>	<u>33.222</u>	<u>51.351</u>	65.353	99.107	25.373	<u>39.432</u>
$EWMA$	53.792	82.799	53.034	82.561	72.673	109.796	48.785	75.090
PCA	77.678	118.355	108.475	165.210	79.607	120.884	57.115	87.187
RMT	77.365	118.210	108.260	165.073	79.904	120.760	56.560	87.032
LW	74.952	114.767	103.983	158.985	80.888	122.122	54.369	83.906
LW^F	49.692	75.555	47.295	71.544	<u>45.710</u>	<u>70.616</u>	52.408	79.599
CCC	43.349	68.233	42.431	67.189	58.278	88.611	39.597	62.977
DCC	40.167	64.257	38.751	62.682	52.667	81.284	37.446	60.321
DCC^{NL}	40.261	66.455	49.351	77.363	80.796	119.188	<u>22.552</u>	44.012
CAB	**18.246**	**27.828**	**29.049**	**44.148**	**14.976**	**22.681**	**12.182**	**18.727**

$F = 250$